Article

Cell

An Essential Role of the Mitochondrial Electron Transport Chain in Cell Proliferation Is to Enable Aspartate Synthesis

Graphical Abstract

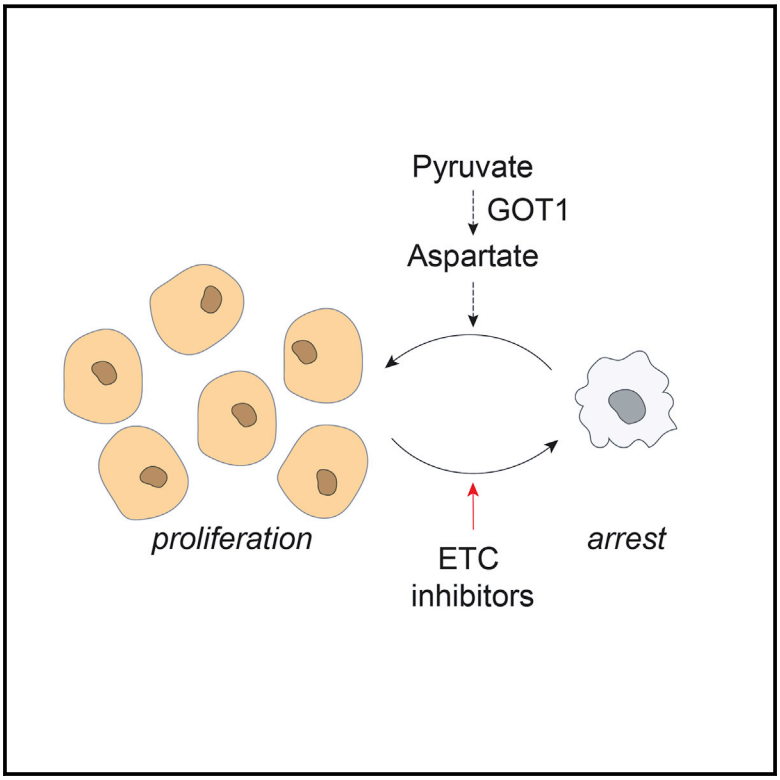

Authors

Kıvanç Birsoy, Tim Wang, Walter W. Chen, Elizaveta Freinkman, Monther Abu-Remaileh, David M. Sabatini

Correspondence

sabatini@wi.mit.edu

In Brief

Aspartate is a limiting metabolite for proliferation in cells with mitochondrial electron transport chain defects.

Highlights

- A CRISPR-Cas9 genetic screen reveals that GOT1 loss kills cells upon ETC inhibition
- In cells with ETC inhibition, GOT1 reverses flux to generate aspartate in the cytosol
- Aspartate is limiting for proliferation in cells with ETC inhibition
- Pyruvate reverses the effects of ETC inhibition by inducing aspartate synthesis

Birsoy et al., 2015, Cell *162*, 540–551
July 30, 2015
http://dx.doi.org/10.1016/j.cell.2015.07.016

CellPress

Cell

Article

An Essential Role of the Mitochondrial Electron Transport Chain in Cell Proliferation Is to Enable Aspartate Synthesis

Kıvanç Birsoy,[1,2,3,4,5] Tim Wang,[1,2,3,4] Walter W. Chen,[1,2,3,4] Elizaveta Freinkman,[1] Monther Abu-Remaileh,[1,2,3,4] and David M. Sabatini[1,2,3,4,*]

[1]Whitehead Institute for Biomedical Research, 9 Cambridge Center, Cambridge, MA 02142, USA
[2]Howard Hughes Medical Institute, Department of Biology, Massachusetts Institute of Technology, Cambridge, MA 02139, USA
[3]Koch Institute for Integrative Cancer Research, 77 Massachusetts Avenue, Cambridge, MA 02139, USA
[4]Broad Institute of Harvard and Massachusetts Institute of Technology, 7 Cambridge Center, Cambridge, MA 02142, USA
[5]Present address: Laboratory of Metabolic Regulation and Genetics, The Rockefeller University, New York, NY 10065, USA
*Correspondence: sabatini@wi.mit.edu
http://dx.doi.org/10.1016/j.cell.2015.07.016

SUMMARY

The mitochondrial electron transport chain (ETC) enables many metabolic processes, but why its inhibition suppresses cell proliferation is unclear. It is also not well understood why pyruvate supplementation allows cells lacking ETC function to proliferate. We used a CRISPR-based genetic screen to identify genes whose loss sensitizes human cells to phenformin, a complex I inhibitor. The screen yielded GOT1, the cytosolic aspartate aminotransferase, loss of which kills cells upon ETC inhibition. GOT1 normally consumes aspartate to transfer electrons into mitochondria, but, upon ETC inhibition, it reverses to generate aspartate in the cytosol, which partially compensates for the loss of mitochondrial aspartate synthesis. Pyruvate stimulates aspartate synthesis in a GOT1-dependent fashion, which is required for pyruvate to rescue proliferation of cells with ETC dysfunction. Aspartate supplementation or overexpression of an aspartate transporter allows cells without ETC activity to proliferate. Thus, enabling aspartate synthesis is an essential role of the ETC in cell proliferation.

INTRODUCTION

The mitochondrial electron transport chain (ETC) consists of four enzyme complexes that transfer electrons from donors like NADH to oxygen, the ultimate electron acceptor. During electron transfer, the ETC pumps protons into the inter-membrane space, generating a gradient across the inner mitochondrial membrane that the F_oF_1 ATPase exploits to drive ATP synthesis (Mitchell, 1961; Nicholls and Budd, 2000; Wallace, 2013). Many metabolic pathways, including glycolysis, the TCA cycle, and beta-oxidation, produce the electron donors that fuel the ETC. In turn, ETC activity impacts a variety of processes beyond energy balance (Pagliarini and Rutter, 2013), such as reactive oxygen species (ROS) production (Bell et al., 2007; Boveris et al., 1972), the redox state (Di Lisa and Ziegler, 2001; Stein and Imai, 2012), mitochondrial membrane potential (Chen et al., 2014), mitochondrial protein import (Geissler et al., 2000), apoptosis (Green and Reed, 1998), and signaling (Chandel, 2014). Diseases caused by genetic defects in the ETC are characterized by diverse pathologies (Koopman et al., 2012), like neurodegeneration (Bender et al., 2006; Swerdlow et al., 1996), myopathy (DiMauro, 2010), and deafness (Kokotas et al., 2007; Raimundo et al., 2012), but in most cases it is unclear how ETC dysfunction leads to the specific symptom and sign.

One consequence of ETC dysfunction is impaired cell proliferation, and human cells in culture arrest upon pharmacological or genetic inhibition of complex I (Fendt et al., 2013; Wheaton et al., 2014) or III (Han et al., 2008; Howell and Sager, 1979). Even though changes in ATP or ROS levels have been suggested to underlie the anti-proliferative effects of ETC inhibition (Wallace, 1999), the exact reason why proliferation requires the ETC is not understood. Interestingly, it has long been known that human cells lacking a functional ETC can proliferate if cultured in supraphysiological concentrations of pyruvate (King and Attardi, 1989). While pyruvate can serve as a biosynthetic substrate or affect the redox state of the cell by promoting the regeneration of NAD^+ (Harris, 1980; Howell and Sager, 1979), why it reverses the suppressive effects of ETC inhibition on cell proliferation is unknown.

Here, through a CRISPR (clustered regularly interspaced short palindromic repeat)-based genetic screen, we discovered that a key function of the ETC required for cell proliferation is to enable the synthesis of aspartate, a proteogenic amino acid that is also a precursor in purine and pyrimidine synthesis (Lane and Fan, 2015). Aspartate becomes limiting upon ETC inhibition and its supplementation, like that of pyruvate, allows cells with defective ETC activity to proliferate. Finally, we find that pyruvate reverses the anti-proliferative effects of ETC inhibition by inducing aspartate synthesis.

RESULTS AND DISCUSSION

A CRISPR-Based Genetic Screen For Metabolic Genes that When Lost Sensitize Human Cells to Phenformin

Pharmacological or genetic inhibition of the ETC greatly suppresses cell proliferation (Santidrian et al., 2013; Wheaton

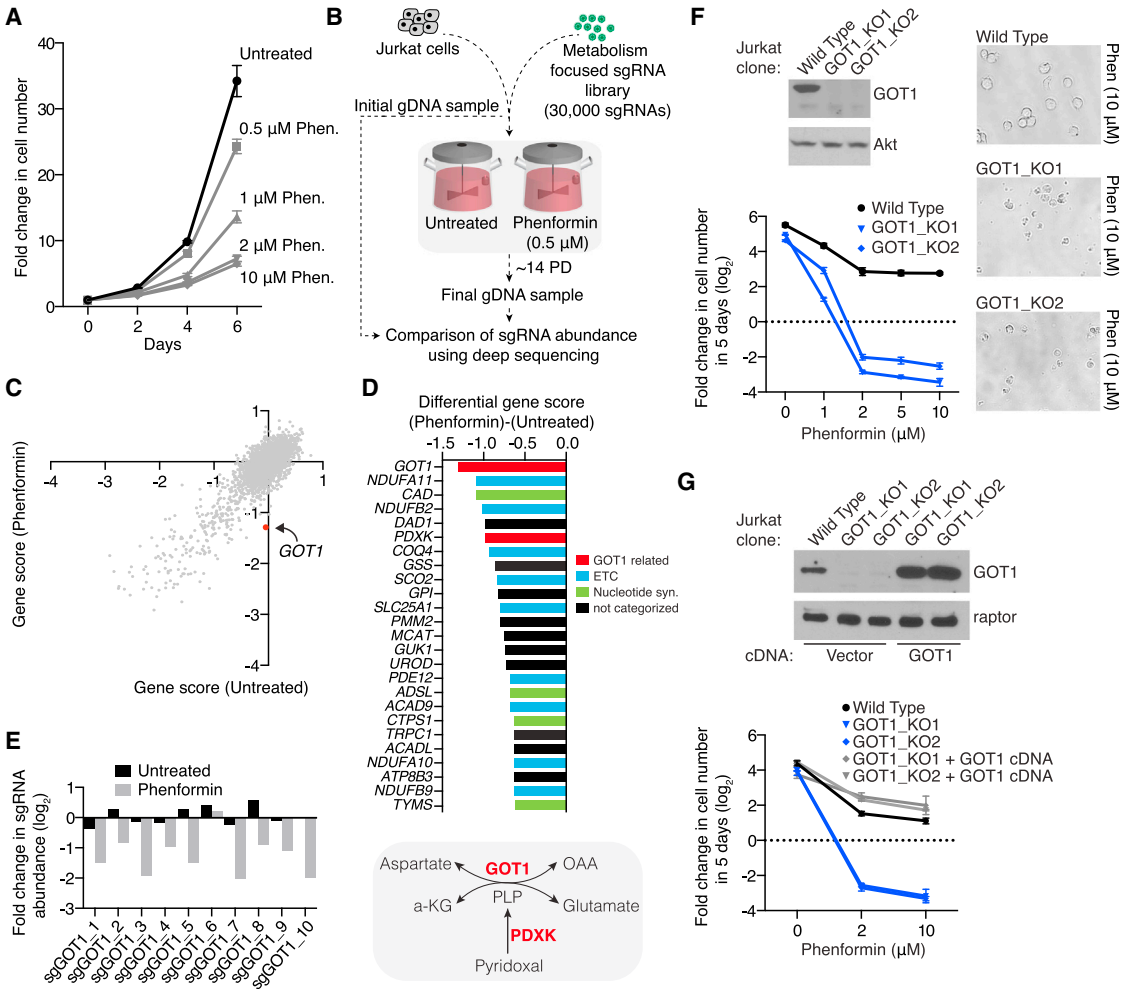

Figure 1. A CRISPR-Based Genetic Screen Identifies Metabolic Genes Whose Loss Sensitizes Human Cells to Phenformin

(A) Dose-dependent effects of phenformin on Jurkat cell proliferation (mean ± SD, n = 3).

(B) Schematic depicting the pooled CRISPR-based screen. PD, Population doublings.

(C) Gene scores in untreated versus phenformin-treated (0.5 μM) Jurkat cells. The gene score is the median $\log_2$ fold change in the abundance of all sgRNAs targeting that gene during the culture period. Most genes, as well as non-targeting control sgRNAs, have similar scores in the presence or absence of phenformin.

(D) Top 25 genes scoring as differentially required upon phenformin treatment (top). Genes linked to the GOT1-catalyzed transamination reaction are indicated in red, the ETC in blue, and to nucleotide biosynthesis in green. The top-scoring gene, GOT1, catalyzes the transamination of aspartate to alpha-ketoglutarate yielding L-glutamate and oxaloacetate (OAA) and requires PLP as a cofactor (bottom).

(E) Changes in abundance in the primary screen of the individual GOT1 sgRNAs in the presence (gray) or absence (black) of phenformin.

(F) GOT1-null cells die upon phenformin treatment. Immunoblot analysis for indicated proteins of wild-type and GOT1-null Jurkat cells (top). Akt was used as a loading control. Fold change in cell number $\log_2$ of wild-type (black) and GOT1-null (blue) Jurkat cells after treatment with indicated phenformin concentrations for 5 days (mean ± SD, n = 3) (bottom). Representative bright-field micrographs of indicated cells after a 5-day phenformin treatment (right).

(G) Expression of an sgRNA-resistant GOT1 cDNA rescues phenformin sensitivity of the GOT1-null Jurkat cells. Immunoblot analysis of wild-type, GOT1-null, and rescued null cells (top). Raptor was used as a loading control. Fold change in cell number $\log_2$ of wild-type (black), GOT1-null (blue), and rescued GOT1-null (gray) cells after a 5-day treatment with indicated phenformin concentrations (mean ± SD, for n = 3) (bottom).

et al., 2014) (Figure 1A), but exactly why is unclear. To study this question, we performed a CRISPR-based negative selection screen for genes whose loss potentiates the anti-proliferative effects of mild ETC inhibition. Such genes should reveal processes that help cells adapt to ETC impairment and thus pinpoint key ETC functions in proliferating cells. Given the central role of mitochondria in metabolism, we generated a library consisting of ~30,000 sgRNAs targeting ~3,000 metabolic enzymes, small molecule transporters, and metabolism-related transcription factors (~10 sgRNA/gene) as well as 500 control sgRNAs in a Cas9-expressing lentiviral vector (Figure 1B). We transduced human Jurkat leukemic T cells with the sgRNA library, and passaged the pool of knockout cells in pyruvate-free RPMI media for 14 population doublings in the presence or absence of 0.5 μM phenformin. This lipophilic biguanide inhibits complex I of the ETC (Birsoy et al., 2014;

Owen et al., 2000; Wheaton et al., 2014) and only mildly slowed proliferation at the concentration used (Figure 1A). As expected for an ETC inhibitor, phenformin dose-dependently suppressed respiration as measured by oxygen consumption (Figure S1D).

Using massively parallel sequencing, we measured the abundances of all the sgRNAs in the vehicle- and phenformin-treated Jurkat cells at the beginning and at the end of the culture period. For each gene, we calculated its score as the median $\log_2$ fold change in the abundance of the 10 sgRNAs targeting the gene. As expected, most genes, as well as the control sgRNAs, scored similarly in the presence or absence of phenformin (Figure 1C).

Among the genes selectively required in the presence of phenformin, were several encoding ETC-related proteins, including complex I subunits (*NDUFA11*, *NDUFB2*, *NDUFA10*, *NDUFB9*), mitochondrial RNA processing and ubiquinone synthesis enzymes (*PDE12* and *COQ4*), and ETC assembly factors (*ACAD9* and *SCO2*) (Figure 1D, Figure S1B). Unlike genes encoding core ETC components, these genes were not essential in the absence of phenformin (Figure S1A). This suggests that they are not absolutely required for ETC function, explaining why their loss synergize with low-dose phenformin. These results are consistent with the previous finding that cells having heteroplasmic mitochondrial DNA mutations that partially impair the ETC are hypersensitive to phenformin (Birsoy et al., 2014).

The best scoring gene in the screen was *GOT1*, which encodes the cytosolic aspartate aminotransferase that is part of the malate-aspartate shuttle for transferring reducing equivalents to the mitochondrial matrix (Figures 1D and 1E). GOT1 catalyzes the reversible transfer of an amino group between aspartate and glutamate, and like other transaminases, requires pyridoxal-5-phosphate (PLP) as a cofactor (Toney, 2014) (Figure 1D). Interestingly, the fourth highest scoring gene, *PDXK*, encodes a pyridoxal kinase, which converts vitamin B6 to PLP (Figure S1C**)**. These data strongly suggest that a GOT1-catalyzed reaction is important for maintaining cellular fitness upon mild phenformin treatment. Given its high score and unexplored role during ETC inhibition, we focused our attention on GOT1.

ETC Inhibition Kills Cells Lacking GOT1

To begin to understand how *GOT1* loss sensitizes cells to phenformin, we used the CRISPR-Cas9 system to generate two clonal Jurkat cell lines in which the GOT1 protein was undetectable (GOT1_KO1 and GOT1_KO2) (Figure 1F). Under normal culture conditions, GOT1-null cells are viable and proliferate at slightly slower rates than wild-type cells (Figure S1E). Consistent with the results of the screen, low doses of phenformin inhibited the proliferation of GOT1-null cells to a much greater extent than that of wild-type cells (Figure 1F). Remarkably, at the higher concentrations of phenformin that strongly repress respiration (Figure S1D), GOT1-null cells arrested and died, while the wild-type counterparts did not (Figure 1F, Figure S1E). Importantly, expression of an sgGOT1-resistant human GOT1 cDNA in the null cells eliminated their hypersensitivity to phenformin (Figure 1G). These findings validate the screening results and reveal that GOT1 loss and phenformin interact synergistically in Jurkat cells.

To ask if GOT1 loss sensitizes other cell types to ETC inhibition, we knocked out GOT1 in human Raji lymphoma and KMS-26 multiple myeloma cells, as well as immortalized mouse embryonic fibroblasts (MEFs) (Figure 2A, Figure S2A). Indeed, all the GOT1-null cells were far more sensitive to phenformin than their wild-type counterparts, indicating a generalizable role for GOT1 in cells treated with phenformin (Figure 2A, Figure S2A).

Finally, inhibition of different complexes of the ETC can have pleiotropic effects on metabolism (Bell et al., 2007; Frezza et al., 2011). This raised the possibility that the sensitizing effect of GOT1 loss might be specific to complex I inhibition or even phenformin treatment, in particular. However, this is not the case because compared to wild-type cells, those lacking GOT1 were substantially more sensitive to other complex I inhibitors (metformin and piericidin) as well as the complex III inhibitor, antimycin (Figure 2B, Figures S2B and S2C). These data indicate that GOT1 loss has a synthetic lethal interaction with ETC dysfunction, independently of which complex is inhibited.

Upon ETC Inhibition GOT1 Reverses Flux and Generates Aspartate

GOT1 is part of the malate-aspartate shuttle (Figure 3A, Figure S3A), but no other component of the shuttle (MDH1, MDH2, SLC25A13, GOT2) scored in the screen (Figure S3B). Given these results, we focused on the reaction mediated by GOT1 itself rather than the overall function of the shuttle in transferring reducing equivalents into the mitochondrial matrix.

In normal cells, GOT1 is thought to use aspartate and alpha-ketoglutarate to make oxaloacetate and glutamate (Safer, 1975). Consistent with GOT1 consuming aspartate, its levels are 4- to 5-fold higher in GOT1-null than wild-type Jurkat cells (Figure 3B) (Son et al., 2013). Aspartate is normally synthesized in the mitochondrial matrix through the sequential actions of MDH2 and GOT2 and then transported to the cytosol for use by GOT1 and other enzymes (Figure 3A). Because MDH2 is an oxidoreductase, the drop in the NAD^+/NADH ratio that occurs upon ETC dysfunction should inhibit MDH2 and thus mitochondrial aspartate synthesis. Indeed, in wild-type Jurkat cells, phenformin caused aspartate levels to fall by ~3-fold (Figure 3B).

As GOT1 is bidirectional, the drop in aspartate levels might allow GOT1 to reverse flux so that in cells with ETC dysfunction GOT1 generates rather than consumes aspartate. If this were the case, ETC inhibition should cause aspartate to drop to a greater extent in GOT1-null than wild-type cells. Indeed, in GOT1-null cells, phenformin treatment leads to an almost complete loss of cellular aspartate (~30-fold reduction) without much effect on other amino acids (Figure 3B). Thus, upon ETC inhibition, cells use a GOT1-dependent pathway to generate aspartate. It is important to note, however, that this pathway does not fully compensate for loss of mitochondrial aspartate synthesis as aspartate is 3-fold lower in cells without a functional ETC (Figure 3B). To understand if aspartate levels also drop upon ETC inhibition in a differentiated cell in vivo, we

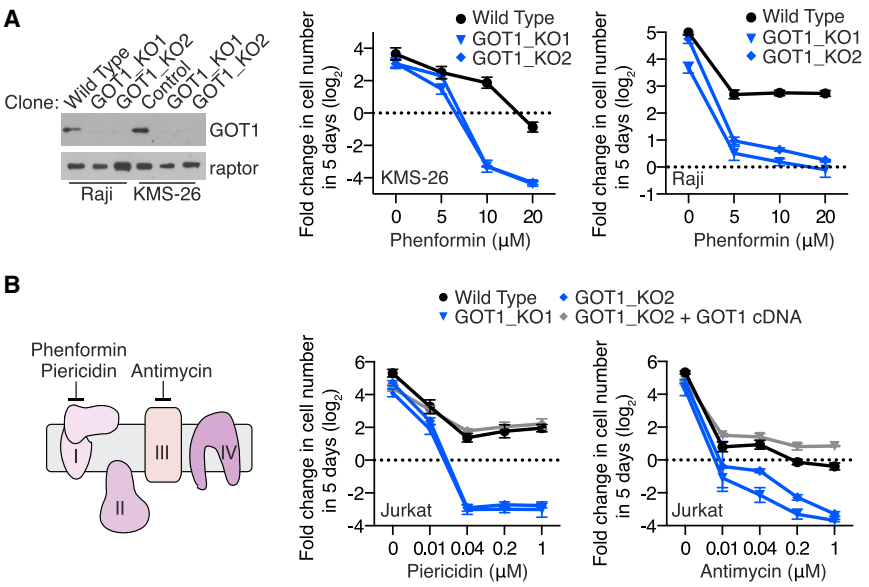

Figure 2. ETC inhibition Kills Cells Lacking GOT1

(A) GOT1 loss sensitizes various human cell types to phenformin treatment. Immunoblot analysis of wild-type and GOT1-null Raji and KMS-26 cells (left). Raptor was used as a loading control. Fold change in cell number $\log_2$ of wild-type (black) and GOT1-null (blue) KMS-26 and Raji cells after a 5-day treatment with indicated phenformin concentrations (mean ± SD, n = 3) (right).

(B) GOT1-null cells die upon ETC dysfunction induced with various ETC inhibitors. Graphical scheme depicting the targets of phenformin (complex I inhibitor), piericidin (complex I inhibitor), and antimycin (complex III inhibitor) (left). Fold change in cell number $\log_2$ of wild-type (black), GOT1-null (blue), and rescued GOT1-null (gray) Jurkat cells after a 5-day treatment with indicated piericidin and antimycin concentrations (mean ± SD, n = 3) (right).

generated a previously reported mouse strain with the heart-specific deletion of mitochondrial transcription factor A (Tfam) (Hansson et al., 2004). Consistent with the severe ETC defect caused by Tfam loss, Tfam knockout hearts had a two-fold lower ratio of aspartate to leucine than wild-type hearts (Figure 3C).

Aspartate Supplementation Enables Cells to Proliferate under Pharmacological ETC Inhibition

Because aspartate is required for the synthesis of proteins as well as purines and pyrimidines (Lane and Fan, 2015), we reasoned that the drop in aspartate levels caused by ETC inhibition might lead to the concomitant suppression of cell proliferation. Consistent with this notion, supplementation of RPMI media with aspartate (10 mM) partially reversed the anti-proliferative effects of phenformin on wild-type cells (Figure 3D). Aspartate addition also prevented the phenformin-induced death of GOT1-null cells and even enabled these cells to proliferate in the presence of the drug (Figure 3D). Given these findings, we re-examined our screen hits and noted that several enzymes scored that use aspartate for purine and pyrimidine synthesis (Figure 1D, Figure S1B).

The aspartate rescue experiments required supplementation of the media with concentrations of aspartate (10 mM) that are higher than those found in standard media (Figure 3D), which is likely a consequence of Jurkat cells having poor aspartate transport. To test this possibility, we cultured GOT1-null cells stably expressing the SLC1A3 glutamate-aspartate transporter in standard RPMI, containing 150 μM aspartate. SLC1A3 imports aspartate (Storck et al., 1992) and is highly expressed in neuronal tissues but not in Jurkat cells (Figures S3C and S3D). Remarkably, SLC1A3 overexpression prevented the death of the GOT1-null cells caused by phenformin (Figure 3E, Figure S3E) and other ETC inhibitors (Figure S3F) and, like high dose aspartate, enabled the proliferation of these cells (Figure 3D, Figures S3E and S3F). Thus, we conclude that upon ETC inhibition, aspartate becomes limiting for maintaining the viability and proliferation of cells.

Metabolic Route for Aspartate Synthesis in Cells with ETC Inhibition

To generate aspartate in cells with ETC inhibition, GOT1 must have a source of oxaloacetate (Figure S4A), which can be made from (1) malate by the cytosolic (MDH1) or mitochondrial (MDH2) malate dehydrogenases; (2) pyruvate by pyruvate carboxylase (PC) in mitochondria; or (3) citrate by ATP-citrate lyase (ACL) in the cytosol. MDH1, MDH2, or PC did not score in our screen as differentially essential upon mild phenformin treatment (Figure S3B, Figure S4B), so we focused on the possible generation of oxaloacetate from citrate upon ETC inhibition. In cells with ETC dysfunction, glutamine is a major source of citrate through the "reductive carboxylation" pathway (Metallo et al., 2012; Mullen et al., 2012). In reductive carboxylation, the mitochondrial citrate carrier (SLC25A1) transports glutamine-derived citrate to the cytosol, where ACL cleaves it into oxaloacetate. Consistent with oxaloacetate being generated from citrate in cells with ETC inhibition, SLC25A1 scored as differentially required in our phenformin screen (Figure 1D). The differential requirement of ACL could not be assessed because it scored as essential under all conditions (Figure S4B), likely because it is required for fatty acid synthesis.

To directly determine how aspartate is made, we measured its generation from [U-^{13}C]-L-glutamine in wild-type and GOT1-null Jurkat cells treated with or without phenformin. Oxidative metabolism of the uniformly labeled glutamine will generate aspartate with four ^{13}C atoms (m+4), while aspartate made by reductive carboxylation will have three ^{13}C atoms (m+3) (Figure 4A). Under normal conditions, we found that oxidative glutamine metabolism was the predominant source of aspartate (~50% of total aspartate pool) in both wild-type and GOT1-null Jurkat cells (Figure 4B). Upon ETC inhibition, aspartate synthesis

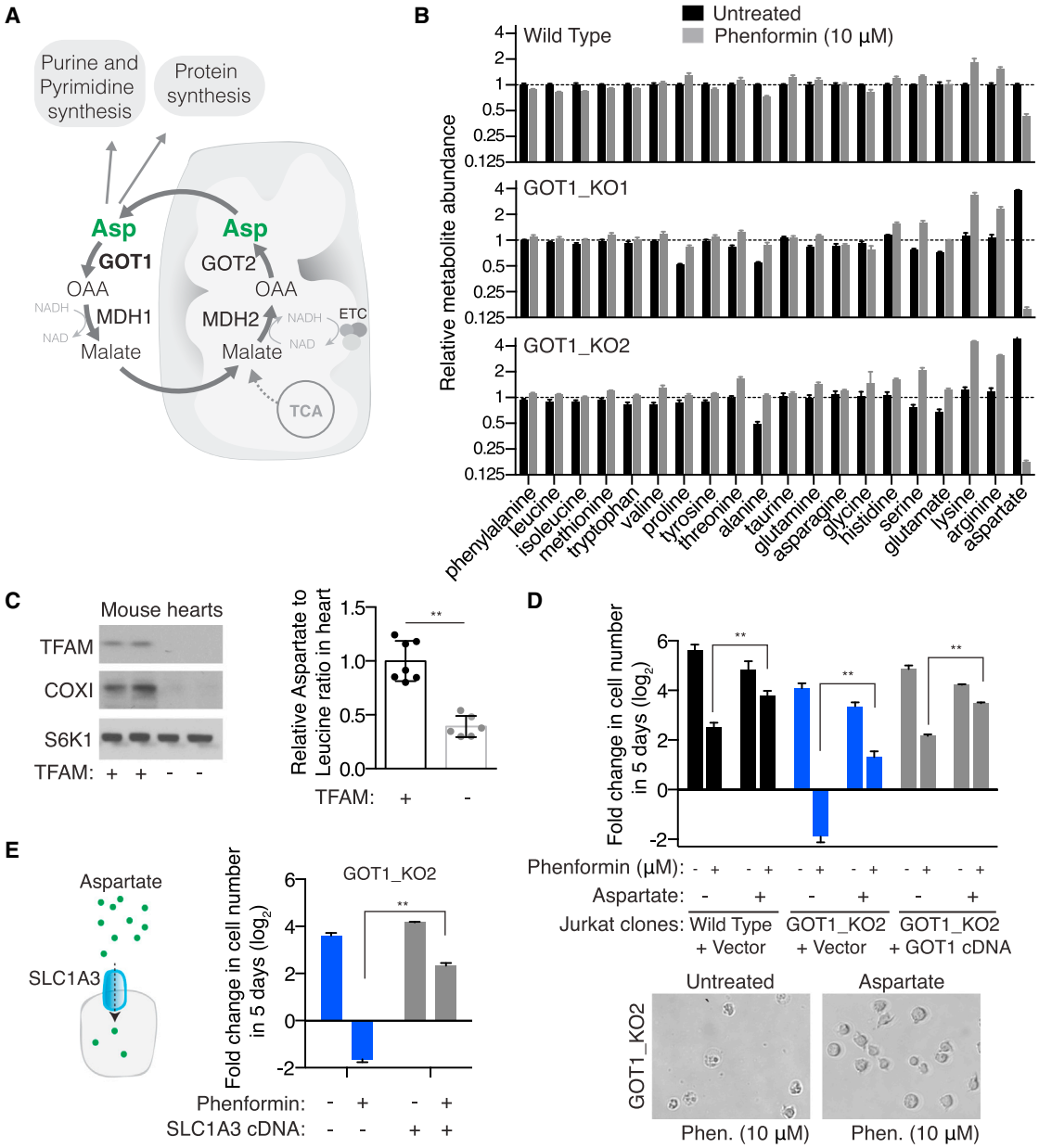

Figure 3. Upon ETC Inhibition, GOT1 Reverses and Generates Aspartate, Which Is Limiting for Cell Proliferation

(A) Schematic depicting the malate-aspartate shuttle. Normally, the malate-aspartate shuttle runs in the forward direction to transfer reducing equivalents across the mitochondrial membrane. GOT1 is part of the malate-aspartate shuttle and consumes aspartate to generate oxaloacetate (OAA). Aspartate produced by mitochondria is a precursor for protein and nucleotide biosynthesis.

(B) Upon ETC inhibition, GOT1 reverses and consumes aspartate. Relative abundance of indicated amino acids in wild-type and GOT1-null Jurkat cells after a 24 hr treatment in the presence (gray) or absence of (black) phenformin (mean ± SD, n = 3). All measurements are relative to untreated wild-type Jurkat cells.

(C) Tfam knockout hearts have a lower ratio of aspartate to leucine than wild-type hearts. Immunoblot analyses of TFAM and COXI in wild-type and TFAM-null murine hearts (left). S6K1 was used as a loading control. Relative ratio of aspartate to leucine in wild-type and TFAM-null mouse hearts (mean ± SD, n = 7 (wild-type) and n = 6 (TFAM-null), **p < 0.05).

(D) Aspartate supplementation rescues death of GOT1-null cells upon ETC inhibition. Fold change in cell number (log_2) of wild-type (black), GOT1-null (blue) and rescued GOT1-null (gray) Jurkat cells in the absence and presence (10 mM) of aspartate after treatment with the indicated phenformin concentrations for 5 days (mean ± SD, n = 3, **p < 0.05) (top). Representative bright-field micrographs of indicated cells after a 5-day phenformin treatment in the absence or presence of aspartate (bottom).

(E) Expression of a glutamate-aspartate transporter (SLC1A3) rescues the phenformin-induced death of GOT1-null cells cultured in standard RPMI media, which contains only 150 μM aspartate. Fold change in cell number (log_2) of GOT1-null (blue) and SLC1A3-overexpressing GOT1-null (gray) Jurkat cells in RPMI (150 μM aspartate) after a 5-day treatment with 10 μM phenformin (mean ± SD, n = 3, **p < 0.05).

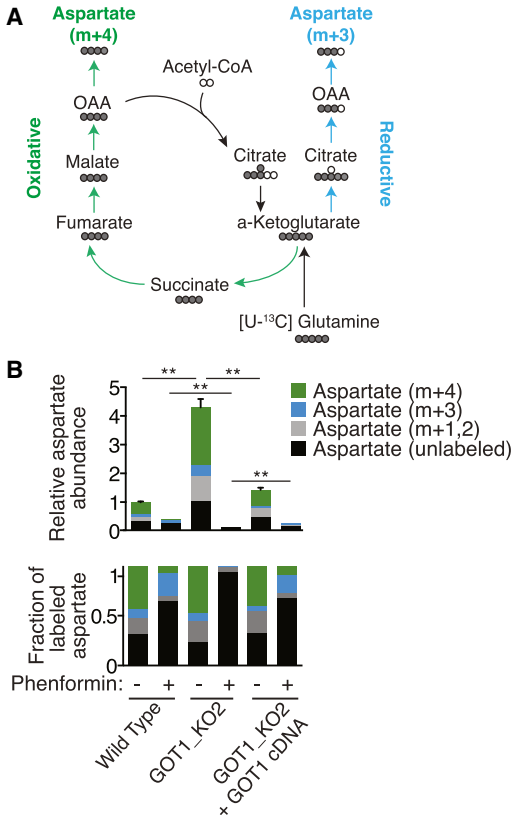

Figure 4. Metabolic Routes of Aspartate Synthesis in Cells with ETC Inhibition

(A) Schematic depicting oxidative and reductive glutamine metabolism pathways. Green and blue arrows indicate oxidative and reductive arms of the TCA cycle, respectively. Filled circles represent ^{13}C atoms derived from [U-^{13}C]-L-glutamine.

(B) Upon ETC inhibition, aspartate is mainly synthesized by reductive metabolism of glutamine in a GOT1-dependent manner. Mass isotopomer analysis of aspartate in wild-type and GOT1-null Jurkat cells cultured for 7 hr with [U-^{13}C]-L-glutamine in the presence or absence of phenformin (10 μM). Aspartate pool sizes (top) and fraction of labeled aspartate derived from labeled glutamine (bottom) for each sample are indicated in separate graphs (mean ± SD, for n = 3, **p < 0.05). OAA, oxaloacetate.

dropped, and what remained came primarily from reductive glutamine metabolism with almost no contribution from the oxidative pathway (Figure 4B). Reductive formation of aspartate completely depends on GOT1 activity, as in phenformin-treated GOT1-null cells there was almost no generation of aspartate or aspartate-derived nucleotide precursors from labeled glutamine (Figure 4B, Figure S4C). These results indicate that upon ETC inhibition cells use the reductive carboxylation of glutamine to fuel compensatory aspartate synthesis via a GOT1-requiring pathway.

Pyruvate Stimulates Aspartate Synthesis in a GOT1-Dependent Fashion

It has long been appreciated that human cells with ETC dysfunction can proliferate when cultured in media containing supra-physiological concentrations of pyruvate (Harris, 1980). Remarkably, pyruvate even enables the proliferation of cells that have deleterious mutations in their mitochondrial DNA or lack it altogether (143B ρ^0 cells) (King and Attardi, 1989). Pyruvate has been hypothesized to act as a biosynthetic substrate or to maintain the cellular redox state in cells with ETC dysfunction via reduction by lactate dehydrogenase, which helps regenerate the NAD^+ that is lost upon ETC inhibition (Harris, 1980; Wilkins et al., 2014). The NAD^+ made through pyruvate reduction should facilitate glycolytic flux and thus ATP production in cells lacking ETC function, but the key metabolic consequence of pyruvate addition that allows such cells to proliferate is unclear.

As both pyruvate and aspartate supplementation enables the proliferation of cells with ETC dysfunction, we explored a possible link between the two by culturing wild-type and GOT1-null cells in the presence or absence of pyruvate and treating them with ETC inhibitors. Consistent with previous reports (Harris, 1980), pyruvate almost completely blocked the anti-proliferative effects of several ETC inhibitors (phenformin, piericidin, and antimycin) on wild-type Jurkat cells (Figure 5A). In contrast, pyruvate had no beneficial effect on the GOT1-null cells (Figure 5A), suggesting that the pyruvate-mediated rescue requires aspartate synthesis via GOT1. Indeed, pyruvate restored aspartate levels to normal in phenformin-treated wild-type cells, but had no effect on aspartate in phenformin-treated GOT1-null cells (Figure 5B). Collectively, these data indicate that a key mechanism through which pyruvate restores the proliferation of cells with ETC inhibition is to promote GOT1-catalyzed aspartate synthesis (Figure 5C).

Metabolic Path of Pyruvate-Induced Aspartate Synthesis

To understand how pyruvate stimulates aspartate synthesis in cells with ETC inhibition, we considered two pathways through which pyruvate might contribute to the aspartate pool. (1) One possibility is that pyruvate carboxylase (PC) directly carboxylates pyruvate into oxaloacetate, which GOT1 then uses to generate aspartate. However, we quickly ruled out this pathway as in PC-null Jurkat cell lines pyruvate still prevented the anti-proliferative effects of ETC inhibitors (Figure S5A). (2) As described earlier, pyruvate can promote the regeneration of NAD^+ in the cytosol. Given this, we hypothesized that NAD^+ might activate the cytosolic malate dehydrogenase (MDH1) to generate oxaloacetate that then drives aspartate synthesis by GOT1. To investigate this possibility, we generated MDH1-null Jurkat cells (MDH1_KO1 and MDH1_KO2) (Figure 6A). In the absence of ETC inhibitors, these cells had similar levels of aspartate as GOT1-null cells, consistent with MDH1 normally consuming the oxaloacetate generated by GOT1 from aspartate (Figure 6B). Upon phenformin treatment, aspartate in the MDH1-null cells dropped to the same level as it did in wild-type cells (Figure 6B). Pyruvate, however, had no effect on the MDH1-null cells: in cells treated with ETC inhibitors it did not stimulate aspartate synthesis or rescue their proliferation (Figures 6A and 6B). Importantly, aspartate supplementation or expression in the null cells of an sgRNA-resistant human MDH1 cDNA reversed this proliferation defect (Figures 6A and 6B, Figure S5C). Our findings suggest a model in which

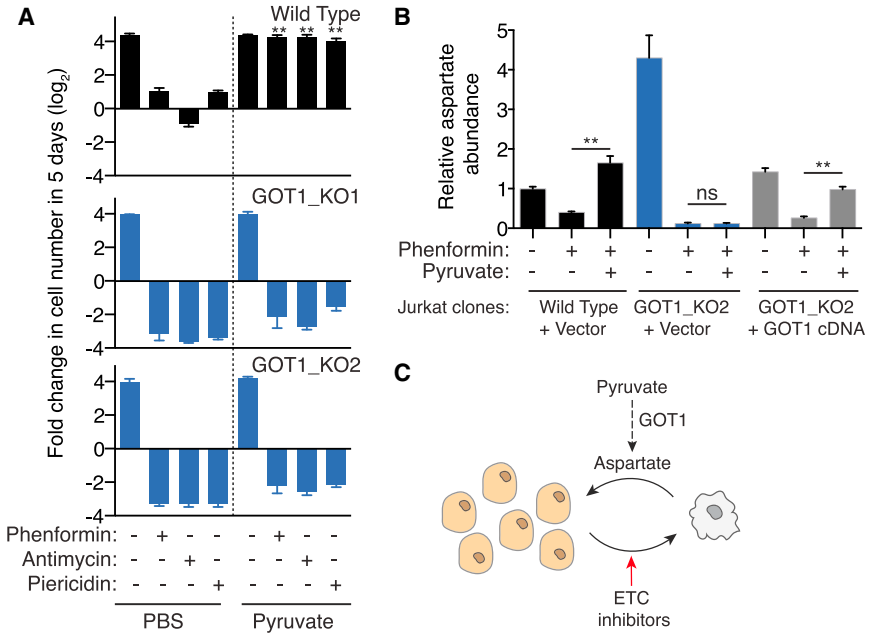

Figure 5. In Cells with ETC Inhibition Pyruvate Stimulates Aspartate Synthesis in a GOT1-Dependent Fashion

(A) Pyruvate cannot rescue death of GOT1-null cells induced by ETC inhibitors. Fold change in cell number (log_2) of wild-type (black) and GOT1-null (blue) Jurkat cells in the presence or absence of pyruvate (1 mM) after treatment with phenformin (10 μM), antimycin (1 μM) and piericidin (1 μM) for 5 days (mean ± SD, n = 3, **p < 0.05).

(B) In cells with ETC inhibition pyruvate addition increases cellular aspartate levels in a GOT1-dependent manner. Relative aspartate levels were measured in wild-type (black), GOT1-null (blue), and rescued GOT1-null (gray) Jurkat cells in the presence (1 mM) or absence of pyruvate after a 24 hr phenformin (10 μM) treatment using LC-MS/MS (mean ± SD, for n = 3, **p < 0.05). All measurements are relative to untreated wild-type Jurkat cells.

(C) Proposed mechanism of pyruvate-mediated rescue of cell proliferation upon ETC inhibition.

pyruvate-induced NAD^+ activates MDH1 to produce oxaloacetate from malate and drive aspartate synthesis via GOT1. In addition, the reductive pathway to oxaloacetate synthesis that operates in the absence of pyruvate (Figure 6C) is still operational, so in the presence of pyruvate there are likely multiple ways of fueling GOT1 for aspartate synthesis (Figure 6C). Supporting the idea that redox balance is upstream of aspartate synthesis, aspartate addition, unlike that of pyruvate, did not restore the NAD/NADH ratio in cells with ETC inhibition (Figure S5B).

Although under normal conditions both GOT1- and MDH1-null cells have high aspartate levels, they behave strikingly differently upon ETC inhibition: aspartate levels become almost undetectable in GOT1-null cells and the cells die, while in MDH1-null cells aspartate and proliferation drop to the same extent as in wild-type cells (Figure 6D). This major difference in aspartate levels upon ETC inhibition is a consequence of the MDH1-null (and also wild-type) cells being able to generate some aspartate even in the absence of pyruvate through the reductive carboxylation pathway described earlier while the GOT1-null cells cannot (Figure 4). In other words, in the absence of ETC function, the loss of GOT1 eliminates all routes to aspartate synthesis while the reductive carboxylation path is still available in the MDH1-null and wild-type cells.

This conclusion also provides a rationale for why MDH1 did not score like GOT1 in our screen, which was performed in RPMI, a pyruvate-free medium (Figure 1B). In the absence of pyruvate and when treated with ETC inhibitors, MDH1-null and wild-type cells have comparable aspartate levels and proliferate equally poorly (Figures 6A and 6B). Interestingly, aspartate levels in wild-type, GOT1-null, and MDH1-null cells treated with ETC inhibitors are a good predictor of whether the cells proliferate, arrest, or die (Figure 6D).

Aspartate Supplementation Enables the Proliferation of Cybrids with Patient-Derived mtDNA Mutations Even in the Absence of Pyruvate

Transmitochondrial cytoplasmic hybrid cells (cybrids) are commonly used to study the mechanisms through which mutations in mitochondrial DNA (mtDNA) impair cellular function (Schon et al., 2012). These cells harbor patient-derived mitochondrial genomes with pathogenic mutations, and, like cells treated with ETC inhibitors, require pyruvate to proliferate in culture (King and Attardi, 1989, 1996). Complex III deficient cybrid cells also require the addition of uridine to the media as complex III is needed for its synthesis (Löffler et al., 1997). To expand upon our work with pharmacological inhibition of the ETC, we asked if aspartate supplementation rescues the proliferation of cells with genetic ETC defects. We used two patient-derived cybrid cells, the first with a homoplasmic microdeletion in the cytochrome *b* subunit of complex III (CYTB) associated with a form of parkinsonism and encephalopathy (De Coo et al., 1999; Rana et al., 2000), and the second with a homoplasmic point mutation in the mitochondrially encoded tRNA lysine (*MT-TK*) associated with myoclonic epilepsy with ragged red fibers (MERRF) (Wallace et al., 1988). To characterize the metabolic needs of these cybrids, as well as cells lacking mtDNA (143B ρ^0), we cultured them in media with or without pyruvate or aspartate. In agreement with previous reports, the ETC-deficient cybrids and ρ^0 cells proliferated in media supplemented with pyruvate (Figure 7A). Consistent with the data obtained with pharmacological inhibitors, pyruvate stimulated aspartate synthesis in the ETC-defective cells (Figure 7B) and aspartate on its own enabled their proliferation (Figure 7A). The pyruvate-mediated rescue requires GOT1 as knocking it out in the ETC-defective cybrids severely impaired their proliferation (Figure 7C). Importantly, aspartate supplementation bypassed the need for GOT1 (Figure 7C).

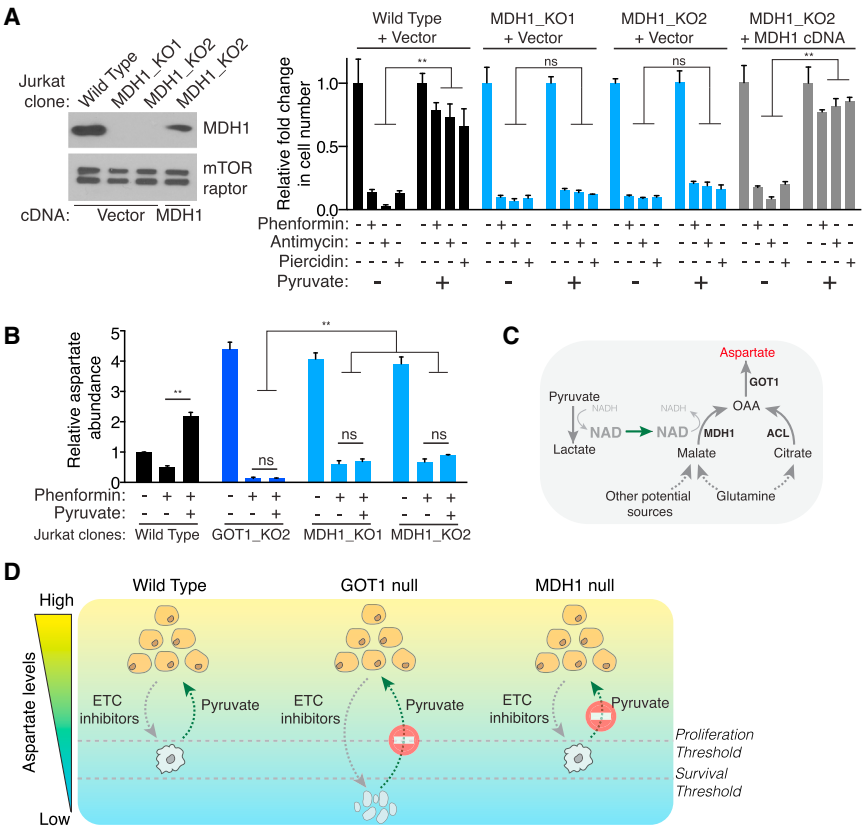

Figure 6. Cells with ETC Inhibition Require MDH1 for Pyruvate to Stimulate Aspartate Synthesis and Enable Proliferation

(A) Pyruvate does not rescue the proliferation of phenformin-treated MDH1-null cells. Immunoblot analysis of wild-type and MDH1-null Jurkat cells along with counterparts expressing an sgRNA-resistant MDH1 cDNA (left). mTOR and Raptor were used as loading controls. Relative fold change in cell number of wild-type (black), MDH1-null (light blue), and rescued MDH1-null (gray) Jurkat cells after a 5-day treatment with phenformin (10 μM), piericidin (1 μM), and antimycin (1 μM) in the presence or absence of pyruvate (1 mM) (mean ± SD, n = 3, **p < 0.05) (right).

(B) The pyruvate-induced increase in aspartate synthesis depends on MDH1. Relative aspartate levels were determined in wild-type (black), GOT1-null (blue), and MDH1-null (light blue) Jurkat cells in the presence or absence of pyruvate (1 mM) after a 24 hr phenformin (10 μM) treatment (mean ± SD, for n = 3, **p < 0.05). All measurements are relative to untreated wild-type Jurkat cells.

(C) Metabolic routes for pyruvate-induced aspartate synthesis under ETC inhibition.

Pyruvate, through the lactate dehydrogenases, regenerates NAD+ in the cytoplasm. This NAD+ can activate the cytoplasmic malate dehydrogenase to provide OAA from malate and drive aspartate synthesis via GOT1. Alternatively, another source for OAA is through ATP-citrate lyase, which catalyzes the conversion of citrate and CoA into acetyl-CoA and OAA in the cytosol. Under ETC inhibition, the latter reaction is likely less dependent on NAD+ and can work even in the absence of pyruvate supplementation. Note that both pathways are dependent on GOT1.

(D) Aspartate levels correlate with cellular health upon ETC inhibition. ETC inhibition leads to a decrease in aspartate levels and inhibits cell proliferation in wild-type cells. The residual aspartate generated by GOT1 is sufficient to maintain viability, as GOT1 loss results in cell death and corresponds to an almost complete depletion of aspartate. Pyruvate addition rescues aspartate levels and proliferation under ETC inhibition in a GOT1- and MDH1-dependent fashion.

To test the sufficiency of aspartate in enabling the proliferation of cells with genetic ETC defects, we stably expressed the glutamate-aspartate SLC1A3 transporter in the CYTB cybrids (Figure 7D). Strikingly, SLC1A3 expression was sufficient to enable the cybrids to proliferate in standard RPMI media, which has a low aspartate concentration (150 μM) and no pyruvate (Figure 7D). To rule out the possibility that SLC1A3 enables proliferation by transporting a molecule other than aspartate, we cultured the cells in aspartate-free RPMI. Now, the SLC1A3-expressing CYTB cybrids failed to proliferate in the absence of pyruvate. Thus, we conclude that aspartate is sufficient to enable the proliferation of cells with a genetic ETC defect.

CONCLUSIONS

Our work suggests that an essential role of the electron transport chain (ETC) in cell proliferation is to enable the biosynthesis of aspartate. Even though ETC inhibition impacts many processes, the supplementation of media with aspartate alone, or the expression in cells of an aspartate transporter, is sufficient to allow ETC-defective cells to proliferate in culture. We also provide an explanation for the classic finding of King and Attardi (King and Attardi, 1989, 1996) that respiration-defective mammalian cells require supra-physiological levels of pyruvate to proliferate. We find that pyruvate, likely by normalizing redox levels (Sullivan, et. al., 2015, this issue of *Cell*), promotes aspartate synthesis to rescue the proliferation of cells with severe ETC defects. It is important to note that although severe ETC inhibition has anti-proliferative effects, the mild ETC inhibition observed in cancer cells having heteroplasmic mtDNA mutations might have beneficial effects on tumorigenesis, likely not by affecting aspartate synthesis, but perhaps by increasing ROS levels (Ishikawa et al., 2008; Kulmacz, 1989; Petros et al., 2005).

As blood aspartate concentrations in children and adults are very low (0–15 μM) (Newgard et al., 2009; Wuu et al., 1988), it is unlikely that in vivo cells with ETC inhibition can take up sufficient aspartate to compensate for the decrease in its synthesis. If future work shows that defective aspartate synthesis contributes to the pathophysiology of diseases characterized by ETC dysfunction, it will be necessary to consider therapies that increase cellular aspartate levels in vivo. One can imagine several strategies for accomplishing this, including delivery of cell-permeable aspartate-releasing pro-drugs or small molecules that indirectly boost aspartate by increasing pyruvate or

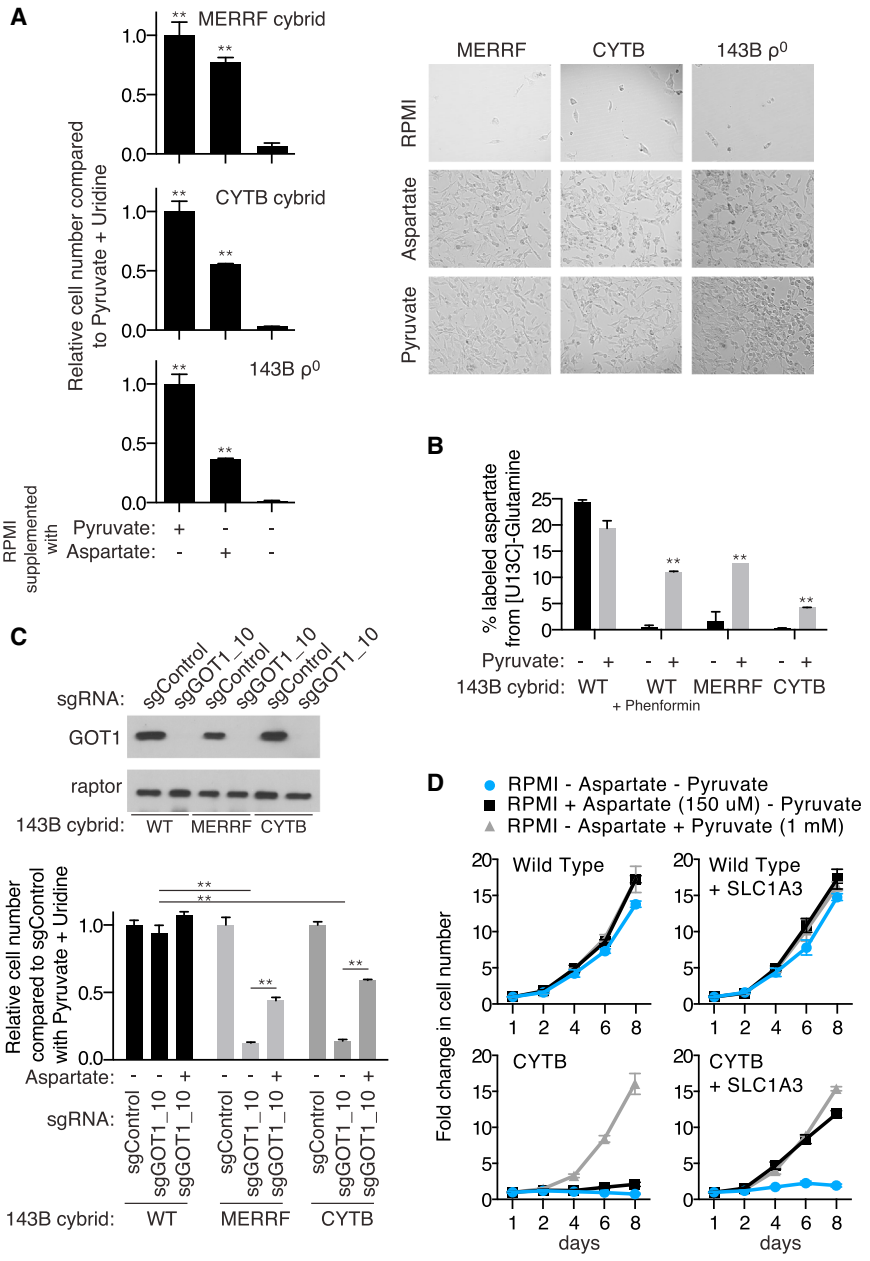

Figure 7. Aspartate Supplementation Enables the Proliferation of Patient-Derived Cybrids with mtDNA Mutations and Replaces the Need for Pyruvate

(A) Aspartate can replace pyruvate in enabling the proliferation of patient-derived mtDNA mutant cybrids and 143B ρ^0 cells devoid of mtDNA. Cell line models of ETC dysfunction were cultured in RPMI (supplemented with 50 μg/ml uridine to bypass the need for complex III in uridine synthesis) with pyruvate (1 mM) or aspartate (10 mM) for 6 days. Relative cell number was determined by normalizing to the pyruvate-supplemented condition. Representative bright-field micrographs of MERRF, CYTB, and 143B ρ^0 cells after 6 days in indicated conditions (right) (mean ± SD, n = 3, $^{**}p < 0.05$).

(B) Pyruvate stimulates aspartate biosynthesis in cybrid cells with ETC dysfunction.

Mass isotopomer analysis of aspartate in wild-type, phenformin-treated wild-type, and ETC-defective cybrid cells cultured for 7 hr with [U-^{13}C]-L-glutamine in the presence or absence of pyruvate (1 mM). The fraction of labeled aspartate from [U-^{13}C]-L-glutamine is indicated (mean ± SD, for n = 3, $^{**}p < 0.05$). OAA, oxaloacetate.

(C) Pyruvate supplementation enables the proliferation of patient-derived cybrid cells in a GOT1-dependent fashion that can be bypassed by aspartate. Immunoblot analysis of wild-type, MERRF, and CYTB cybrid cells expressing sgControl and sgGOT1 (top). Raptor was used as a loading control. Cell line models of ETC dysfunction expressing sgControl or sgGOT1 were cultured in RPMI (supplemented with uridine (50 μg/ml) and pyruvate (1 mM)) with or without aspartate (10 mM) for 6 days (bottom). Relative cell number was determined by normalizing to sgControl expressing cell line (mean ± SD, for n = 3, $^{**}p < 0.05$).

(D) SLC1A3 overexpression enables CYTB cells to proliferate in standard RPMI media without pyruvate addition. Fold changes in cell number over time of 143B wild-type, CYTB cybrid cells, and their SLC1A3-expressing counterparts when cultured in RPMI media lacking aspartate and pyruvate (blue), or supplemented with aspartate (150 μM) (black) or pyruvate (1 mM) (gray) (mean ± SD, n = 3).

the NAD$^+$/NADH ratio. Two case reports showing that pyruvate treatment of patients with mitochondrial disease has some clinical benefit (Fujii et al., 2014; Saito et al., 2012) supports the notion that the pyruvate-aspartate axis may be of therapeutic interest. Efforts to explore this possibility are warranted given that current therapies for these diseases are of limited efficacy (Pfeffer et al., 2012).

EXPERIMENTAL PROCEDURES

CRISPR-Based Screen

The metabolism-focused sgRNA library was designed and performed as previously described (Wang et al., 2014). Oligonucleotides for sgRNAs were synthesized by CustomArray Inc. and amplified by PCR (Wang et al., 2014). Gene scores of all the metabolic genes in the screen can be found in Table S1.

Proliferation Assays

Indicated cell lines were cultured in replicates of three in 96-well plates at 2–3,000 cells per well in 200 μl RPMI base media under the conditions described in each experiment, and a separate group of 3 wells was also plated for each cell line with no treatment for an initial time point. After 5 hr (untreated cells for initial time point) or after 5 days (with varying treatment conditions), 40 μl of Cell Titer Glo reagent (Promega) was added to each well, mixed briefly, and the luminescence read on a Luminometer (Molecular Devices). For each well, the fold change in luminescence relative to the initial luminescence was measured and reported in a $\log_2$ scale. For

Figure 6, relative fold change in luminescence relative to initial was calculated.

Cell Counting Assays

Cybrids or 143B ρ0 cells were plated in triplicate in 12 well plates at 5,000–20,000 cells per well in 1.5 ml as described in each experiment. After 6 days, the entire contents of the well was trypsinized and counted using a Beckman Z2 Coulter Counter with a size selection setting of 8–30 μm.

Generation of Knockout and cDNA Overexpression Cell Lines

sgRNAs (oligonucleotide sequences are indicated above) were cloned into lentiCRISPR-v1 linearized with BsmBI by Gibson Assembly (NEB). sgRNA expressing vector along with lentiviral packaging vectors Delta-VPR and CMV VSV-G were transfected into HEK293T cells using the XTremeGene 9 transfection reagent (Roche). Similarly, for overexpression cell lines, cDNA vectors along with retroviral packaging vectors gag-pol and CMV VSV-G were transfected into HEK293T cells. Media was changed 24 hr after transfection. The virus-containing supernatant was collected 48 and 72 hr after transfection and passed through a 0.45 μm filter to eliminate cells. Target cells in 6-well tissue culture plates were infected in media containing 8 μg/ml of polybrene and a spin infection was performed by centrifugation at 2,200 rpm for 1 hr. Post-infection, virus was removed and cells were selected with puromycin or blasticidin. For knockout cells, after selection, cells were single-cell sorted with a flow cytometer into the wells of a 96-well plate containing 200 μl of RPMI supplemented with 20% FBS. Cells were grown for 2 weeks, and the resultant colonies were trypsinized and expanded. Clones were validated for loss of the relevant protein via immunoblotting.

Metabolite Profiling and Isotope Tracing

LC/MS analyses were conducted on a QExactive benchtop orbitrap mass spectrometer equipped with an Ion Max source and a HESI II probe, which was coupled to a Dionex UltiMate 3000 UPLC system (Thermo Fisher Scientific, San Jose, CA). External mass calibration was performed using the standard calibration mixture every 7 days.

For metabolite profiling experiments, Jurkat cells (2 million per sample) were incubated with 10 μM phenformin for 24 hr. Similarly, for glutamine tracing experiments, Jurkat cells (2 million per sample) were incubated with 10 μM phenformin for 18 hr; the cells were spun down and media was replaced with RPMI supplemented with 1 mM [U-^{13}C]-L-glutamine for 7 hr. Polar metabolites were extracted using 1 ml of ice-cold 80% methanol with 10 ng/ml valine-d_8 as an internal standard. After a 10 min vortex and centrifugation for 10 min at 4°C at 10,000 *g*, samples were dried under nitrogen gas. Dried samples were stored at −80°C and then resuspended in 100 μl water; 1 μl of each sample was injected onto a ZIC-pHILIC 2.1 × 150 mm (5 μm particle size) column (EMD Millipore). Buffer A was 20 mM ammonium carbonate, 0.1% ammonium hydroxide; buffer B was acetonitrile. The chromatographic gradient was run at a flow rate of 0.150 ml/min as follows: 0–20 min.: linear gradient from 80% to 20% B; 20–20.5 min.: linear gradient from 20% to 80% B; 20.5–28 min.: hold at 80% B. The mass spectrometer was operated in full-scan, polarity switching mode with the spray voltage set to 3.0 kV, the heated capillary held at 275°C, and the HESI probe held at 350°C. The sheath gas flow was set to 40 units, the auxiliary gas flow was set to 15 units, and the sweep gas flow was set to 1 unit. The MS data acquisition was performed in a range of 70–1000 m/z, with the resolution set at 70,000, the AGC target at 10^6, and the maximum injection time at 80 msec. Relative quantitation of polar metabolites was performed with XCalibur QuanBrowser 2.2 (Thermo Fisher Scientific) using a 5 ppm mass tolerance and referencing an in-house library of chemical standards.

SUPPLEMENTAL INFORMATION

Supplemental Information includes Supplemental Experimental Procedures, five figures, and one table and can be found with this article online at http://dx.doi.org/10.1016/j.cell.2015.07.016.

AUTHOR CONTRIBUTIONS

K.B. and D.M.S. initiated the project and designed the research plan. T.W. designed the sgRNA library. E.F. performed mass spectrometry measurements. W.W.C. helped with mouse experiments. M.A.-R. generated GOT1-null MEFs. K.B. wrote the manuscript and D.M.S. edited it.

ACKNOWLEDGMENTS

We thank all members of Sabatini Lab, particularly Andrew Mullen, for helpful suggestions; C. Moraes, I.F.M. de Coo, Doug Wallace, Navdeep Chandel, and Giovanni Manfredi for providing WT 143B, CYTB 143B, 143B Rho, and MERRF 143B cell lines; and Dan Gui and Lucas Sullivan for NAD measurements. This work was supported by NIH (CA103866 and AI047389) grants to D.M.S., and the Jane Coffin Childs Memorial Fund Fellowship and Leukemia and Lymphoma Society Special Fellow Award to K.B. D.M.S. is an investigator of the Howard Hughes Medical Institute.

Received: June 1, 2015
Revised: July 5, 2015
Accepted: July 8, 2015
Published: July 30, 2015

REFERENCES

Barretina, J., Caponigro, G., Stransky, N., Venkatesan, K., Margolin, A.A., Kim, S., Wilson, C.J., Lehár, J., Kryukov, G.V., Sonkin, D., et al. (2012). The Cancer Cell Line Encyclopedia enables predictive modelling of anticancer drug sensitivity. Nature *483*, 603–607.

Bell, E.L., Klimova, T.A., Eisenbart, J., Moraes, C.T., Murphy, M.P., Budinger, G.R., and Chandel, N.S. (2007). The Qo site of the mitochondrial complex III is required for the transduction of hypoxic signaling via reactive oxygen species production. J. Cell Biol. *177*, 1029–1036.

Bender, A., Krishnan, K.J., Morris, C.M., Taylor, G.A., Reeve, A.K., Perry, R.H., Jaros, E., Hersheson, J.S., Betts, J., Klopstock, T., et al. (2006). High levels of mitochondrial DNA deletions in substantia nigra neurons in aging and Parkinson disease. Nat. Genet. *38*, 515–517.

Birsoy, K., Possemato, R., Lorbeer, F.K., Bayraktar, E.C., Thiru, P., Yucel, B., Wang, T., Chen, W.W., Clish, C.B., and Sabatini, D.M. (2014). Metabolic determinants of cancer cell sensitivity to glucose limitation and biguanides. Nature *508*, 108–112.

Boveris, A., Oshino, N., and Chance, B. (1972). The cellular production of hydrogen peroxide. Biochem. J. *128*, 617–630.

Chandel, N.S. (2014). Mitochondria as signaling organelles. BMC Biol. *12*, 34.

Chen, W.W., Birsoy, K., Mihaylova, M.M., Snitkin, H., Stasinski, I., Yucel, B., Bayraktar, E.C., Carette, J.E., Clish, C.B., Brummelkamp, T.R., et al. (2014). Inhibition of ATPIF1 ameliorates severe mitochondrial respiratory chain dysfunction in mammalian cells. Cell Rep. *7*, 27–34.

Consortium, G.T.; GTEx Consortium (2013). The Genotype-Tissue Expression (GTEx) project. Nat. Genet. *45*, 580–585.

De Coo, I.F., Renier, W.O., Ruitenbeek, W., Ter Laak, H.J., Bakker, M., Schägger, H., Van Oost, B.A., and Smeets, H.J. (1999). A 4-base pair deletion in the mitochondrial cytochrome b gene associated with parkinsonism/MELAS overlap syndrome. Ann. Neurol. *45*, 130–133.

Di Lisa, F., and Ziegler, M. (2001). Pathophysiological relevance of mitochondria in NAD(+) metabolism. FEBS Lett. *492*, 4–8.

DiMauro, S. (2010). Pathogenesis and treatment of mitochondrial myopathies: recent advances. Acta Myol. *29*, 333–338.

Fendt, S.M., Bell, E.L., Keibler, M.A., Davidson, S.M., Wirth, G.J., Fiske, B., Mayers, J.R., Schwab, M., Bellinger, G., Csibi, A., et al. (2013). Metformin decreases glucose oxidation and increases the dependency of prostate cancer cells on reductive glutamine metabolism. Cancer Res. *73*, 4429–4438.

Frezza, C., Zheng, L., Folger, O., Rajagopalan, K.N., MacKenzie, E.D., Jerby, L., Micaroni, M., Chaneton, B., Adam, J., Hedley, A., et al. (2011). Haem oxygenase is synthetically lethal with the tumour suppressor fumarate hydratase. Nature *477*, 225–228.

Fujii, T., Nozaki, F., Saito, K., Hayashi, A., Nishigaki, Y., Murayama, K., Tanaka, M., Koga, Y., Hiejima, I., and Kumada, T. (2014). Efficacy of pyruvate therapy in patients with mitochondrial disease: a semi-quantitative clinical evaluation study. Mol. Genet. Metab. *112*, 133–138.

Geissler, A., Krimmer, T., Bömer, U., Guiard, B., Rassow, J., and Pfanner, N. (2000). Membrane potential-driven protein import into mitochondria. The sorting sequence of cytochrome b(2) modulates the deltapsi-dependence of translocation of the matrix-targeting sequence. Mol. Biol. Cell *11*, 3977–3991.

Green, D.R., and Reed, J.C. (1998). Mitochondria and apoptosis. Science *281*, 1309–1312.

Han, Y.H., Kim, S.H., Kim, S.Z., and Park, W.H. (2008). Antimycin A as a mitochondrial electron transport inhibitor prevents the growth of human lung cancer A549 cells. Oncol. Rep. *20*, 689–693.

Hansson, A., Hance, N., Dufour, E., Rantanen, A., Hultenby, K., Clayton, D.A., Wibom, R., and Larsson, N.G. (2004). A switch in metabolism precedes increased mitochondrial biogenesis in respiratory chain-deficient mouse hearts. Proc. Natl. Acad. Sci. USA *101*, 3136–3141.

Harris, M. (1980). Pyruvate blocks expression of sensitivity to antimycin A and chloramphenicol. Somatic Cell Genet. *6*, 699–708.

Howell, N., and Sager, R. (1979). Cytoplasmic genetics of mammalian cells: conditional sensitivity to mitochondrial inhibitors and isolation of new mutant phenotypes. Somatic Cell Genet. *5*, 833–845.

Ishikawa, K., Takenaga, K., Akimoto, M., Koshikawa, N., Yamaguchi, A., Imanishi, H., Nakada, K., Honma, Y., and Hayashi, J. (2008). ROS-generating mitochondrial DNA mutations can regulate tumor cell metastasis. Science *320*, 661–664.

King, M.P., and Attardi, G. (1989). Human cells lacking mtDNA: repopulation with exogenous mitochondria by complementation. Science *246*, 500–503.

King, M.P., and Attardi, G. (1996). Isolation of human cell lines lacking mitochondrial DNA. Methods Enzymol. *264*, 304–313.

Kokotas, H., Petersen, M.B., and Willems, P.J. (2007). Mitochondrial deafness. Clin. Genet. *71*, 379–391.

Koopman, W.J., Willems, P.H., and Smeitink, J.A. (2012). Monogenic mitochondrial disorders. N. Engl. J. Med. *366*, 1132–1141.

Kulmacz, R.J. (1989). Concerted loss of cyclooxygenase and peroxidase activities from prostaglandin H synthase upon proteolytic attack. Prostaglandins *38*, 277–288.

Lane, A.N., and Fan, T.W. (2015). Regulation of mammalian nucleotide metabolism and biosynthesis. Nucleic Acids Res. *43*, 2466–2485.

Löffler, M., Jöckel, J., Schuster, G., and Becker, C. (1997). Dihydroorotat-ubiquinone oxidoreductase links mitochondria in the biosynthesis of pyrimidine nucleotides. Mol. Cell. Biochem. *174*, 125–129.

Metallo, C.M., Gameiro, P.A., Bell, E.L., Mattaini, K.R., Yang, J., Hiller, K., Jewell, C.M., Johnson, Z.R., Irvine, D.J., Guarente, L., et al. (2012). Reductive glutamine metabolism by IDH1 mediates lipogenesis under hypoxia. Nature *481*, 380–384.

Mitchell, P. (1961). Coupling of phosphorylation to electron and hydrogen transfer by a chemi-osmotic type of mechanism. Nature *191*, 144–148.

Mullen, A.R., Wheaton, W.W., Jin, E.S., Chen, P.H., Sullivan, L.B., Cheng, T., Yang, Y., Linehan, W.M., Chandel, N.S., and DeBerardinis, R.J. (2012). Reductive carboxylation supports growth in tumour cells with defective mitochondria. Nature *481*, 385–388.

Newgard, C.B., An, J., Bain, J.R., Muehlbauer, M.J., Stevens, R.D., Lien, L.F., Haqq, A.M., Shah, S.H., Arlotto, M., Slentz, C.A., et al. (2009). A branched-chain amino acid-related metabolic signature that differentiates obese and lean humans and contributes to insulin resistance. Cell Metab. *9*, 311–326.

Nicholls, D.G., and Budd, S.L. (2000). Mitochondria and neuronal survival. Physiol. Rev. *80*, 315–360.

Owen, M.R., Doran, E., and Halestrap, A.P. (2000). Evidence that metformin exerts its anti-diabetic effects through inhibition of complex 1 of the mitochondrial respiratory chain. Biochem. J. *348*, 607–614.

Pagliarini, D.J., and Rutter, J. (2013). Hallmarks of a new era in mitochondrial biochemistry. Genes Dev. *27*, 2615–2627.

Petros, J.A., Baumann, A.K., Ruiz-Pesini, E., Amin, M.B., Sun, C.Q., Hall, J., Lim, S., Issa, M.M., Flanders, W.D., Hosseini, S.H., et al. (2005). mtDNA mutations increase tumorigenicity in prostate cancer. Proc. Natl. Acad. Sci. USA *102*, 719–724.

Pfeffer, G., Majamaa, K., Turnbull, D.M., Thorburn, D., and Chinnery, P.F. (2012). Treatment for mitochondrial disorders. Cochrane Database Syst. Rev. *4*, CD004426.

Raimundo, N., Song, L., Shutt, T.E., McKay, S.E., Cotney, J., Guan, M.X., Gilliland, T.C., Hohuan, D., Santos-Sacchi, J., and Shadel, G.S. (2012). Mitochondrial stress engages E2F1 apoptotic signaling to cause deafness. Cell *148*, 716–726.

Rana, M., de Coo, I., Diaz, F., Smeets, H., and Moraes, C.T. (2000). An out-of-frame cytochrome b gene deletion from a patient with parkinsonism is associated with impaired complex III assembly and an increase in free radical production. Ann. Neurol. *48*, 774–781.

Safer, B. (1975). The Metabolic Significance of the Malate-Aspartate Cycle in Heart. Circ. Res. *37*, 527–533.

Saito, K., Kimura, N., Oda, N., Shimomura, H., Kumada, T., Miyajima, T., Murayama, K., Tanaka, M., and Fujii, T. (2012). Pyruvate therapy for mitochondrial DNA depletion syndrome. Biochim. Biophys. Acta *1820*, 632–636.

Santidrian, A.F., Matsuno-Yagi, A., Ritland, M., Seo, B.B., LeBoeuf, S.E., Gay, L.J., Yagi, T., and Felding-Habermann, B. (2013). Mitochondrial complex I activity and NAD+/NADH balance regulate breast cancer progression. J. Clin. Invest. *123*, 1068–1081.

Schon, E.A., DiMauro, S., and Hirano, M. (2012). Human mitochondrial DNA: roles of inherited and somatic mutations. Nat. Rev. Genet. *13*, 878–890.

Son, J., Lyssiotis, C.A., Ying, H., Wang, X., Hua, S., Ligorio, M., Perera, R.M., Ferrone, C.R., Mullarky, E., Shyh-Chang, N., et al. (2013). Glutamine supports pancreatic cancer growth through a KRAS-regulated metabolic pathway. Nature *496*, 101–105.

Stein, L.R., and Imai, S. (2012). The dynamic regulation of NAD metabolism in mitochondria. Trends Endocrinol. Metab. *23*, 420–428.

Storck, T., Schulte, S., Hofmann, K., and Stoffel, W. (1992). Structure, expression, and functional analysis of a Na(+)-dependent glutamate/aspartate transporter from rat brain. Proc. Natl. Acad. Sci. USA *89*, 10955–10959.

Sullivan, L.B., Gui, D.Y., Hosios, A.M., Bush, L.N., Freinkman, E., and Vander Heiden, M.G. (2015). Supporting Aspartate Biosynthesis Is an Essential Function of Respiration in Proliferating Cells. Cell *162*, this issue, 552–563.

Swerdlow, R.H., Parks, J.K., Miller, S.W., Tuttle, J.B., Trimmer, P.A., Sheehan, J.P., Bennett, J.P., Jr., Davis, R.E., and Parker, W.D., Jr. (1996). Origin and functional consequences of the complex I defect in Parkinson's disease. Ann. Neurol. *40*, 663–671.

Toney, M.D. (2014). Aspartate aminotransferase: an old dog teaches new tricks. Arch. Biochem. Biophys. *544*, 119–127.

Wallace, D.C. (1999). Mitochondrial diseases in man and mouse. Science *283*, 1482–1488.

Wallace, D.C. (2013). A mitochondrial bioenergetic etiology of disease. J. Clin. Invest. *123*, 1405–1412.

Wallace, D.C., Zheng, X.X., Lott, M.T., Shoffner, J.M., Hodge, J.A., Kelley, R.I., Epstein, C.M., and Hopkins, L.C. (1988). Familial mitochondrial encephalomyopathy (MERRF): genetic, pathophysiological, and biochemical characterization of a mitochondrial DNA disease. Cell *55*, 601–610.

Wang, T., Wei, J.J., Sabatini, D.M., and Lander, E.S. (2014). Genetic screens in human cells using the CRISPR-Cas9 system. Science *343*, 80–84.

Wheaton, W.W., Weinberg, S.E., Hamanaka, R.B., Soberanes, S., Sullivan, L.B., Anso, E., Glasauer, A., Dufour, E., Mutlu, G.M., Budigner, G.S., and Chandel, N.S. (2014). Metformin inhibits mitochondrial complex I of cancer cells to reduce tumorigenesis. eLife *3*, e02242.

Wilkins, H.M., Carl, S.M., and Swerdlow, R.H. (2014). Cytoplasmic hybrid (cybrid) cell lines as a practical model for mitochondriopathies. Redox biol. *2*, 619–631.

Wuu, J.A., Wen, L.Y., Chuang, T.Y., and Chang, G.G. (1988). Amino acid concentrations in serum and aqueous humor from subjects with extreme myopia or senile cataract. Clin. Chem. *34*, 1610–1613.

Cell

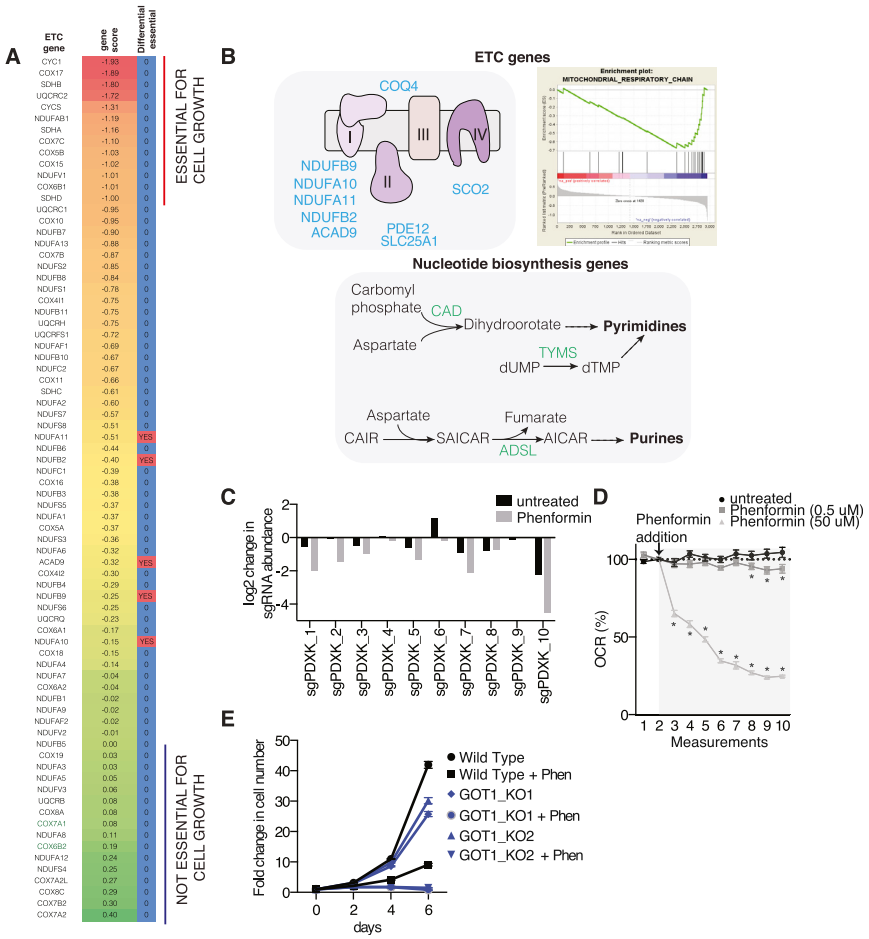

Figure S1. Identification of Metabolic Genes Whose Loss Sensitizes Human Cells to Phenformin, Related to Figure 1

(A) Gene scores for individual electron transport chain components in the absence of phenformin. ETC components with a gene score less than −1 indicates essentiality for cell growth in RPMI media. Right column indicates if ETC components also scored as differentially essential (highlighted in red) upon phenformin treatment.

(B) ETC components (top) and nucleotide biosynthesis (bottom) genes that are differentially essential for cell proliferation with phenformin treatment. Gene set enrichment analysis (GSEA) for the metabolic genes ranked based on their score in the CRISPR-based screen (right).

(C) Changes in abundances in the primary screen for individual PDXK sgRNAs in the presence (gray) or absence (black) of phenformin.

(D) Phenformin inhibits oxygen consumption of wild-type and GOT1-null Jurkat cells. Oxygen consumption was measured using the XF-24 Seahorse Extracellular Flux Analyzer. The measurements were displayed as percent OCR before phenformin injection for each cell line.

(E) Effect of phenformin (10 μM) on the proliferation of wild-type and GOT1-null Jurkat cells (mean ± SD, for n = 3).

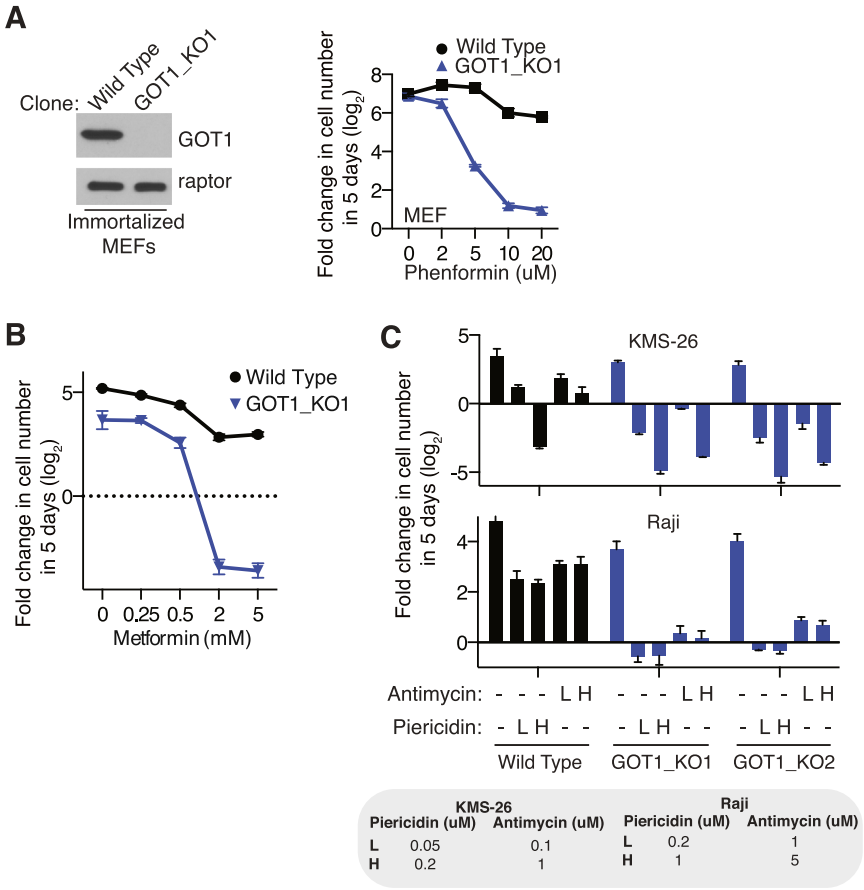

Figure S2. GOT1 Loss Kills Cells upon ETC Inhibition, Related to Figure 2

(A) GOT1 loss sensitizes immortalized mouse embryonic fibroblasts (MEF) to phenformin. Immunoblot analysis of wild-type and GOT1-null MEFs (left). Raptor was used as a loading control. Fold change in cell number (log_2) of wild-type (black) and GOT1-null (blue) MEFs after a 5-day treatment with indicated phenformin concentrations in DMEM with pyruvate (mean ± SD, n = 3) (right). The presence of pyruvate in the media explains why phenformin has weaker effects on MEFs than the human cells used in this study.

(B) GOT1-null cells die upon ETC inhibition with metformin. Fold change in cell number (log_2) of wild-type (black) and GOT1-null (blue) Jurkat cells after a 5-day treatment with indicated metformin concentrations (mean ± SD, n = 3) (right).

(C) GOT1-null KMS-26 and Raji cells die upon ETC inhibition with other mitochondrial toxins besides phenformin. Fold change in cell number (log_2) of wild-type (black) and GOT1-null (blue) KMS-26 (top) and Raji (bottom) cells after a 5-day treatment with indicated antimycin or piericidin concentrations (mean ± SD, n = 3) (right).

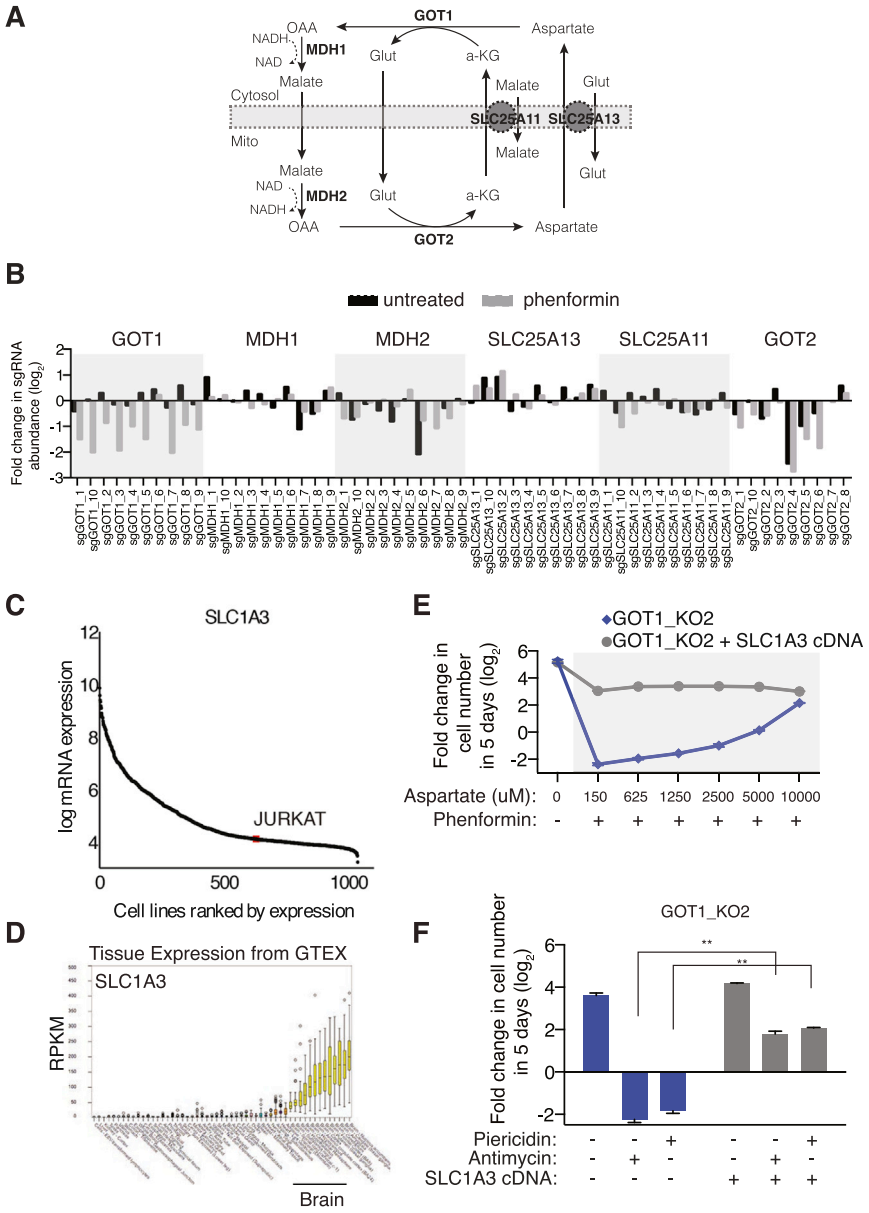

Figure S3. Expression of SLC1A3, a Glutamate-Aspartate Transporter, Rescues the Phenformin-Induced Death of GOT1 Null Cells, Related to Figure 3

(A) Detailed depiction of the malate-aspartate shuttle components and direction of the shuttle under normal conditions.

(B) Changes in abundance in the primary screen for individual sgRNAs (10 sgRNAs for each gene) targeting malate-aspartate shuttle components in the presence (gray) or absence (black) of phenformin.

(C) SLC1A3 mRNA expression in cancer cell lines (obtained from Cancer Cell line Encyclopedia (CCLE) (Barretina et al., 2012).

(D) SLC1A3 mRNA expression in human tissues (obtained from GTEx) (Consortium, 2013).

(E) Expression of a glutamate-aspartate transporter (SLC1A3) rescues the phenformin-induced death of GOT1-null cells at different aspartate concentrations. Fold change in cell number (log_2) of GOT1-null (blue) and SLC1A3-overexpressing GOT1-null (gray) Jurkat cells in RPMI (150 μM aspartate) after a 5-day treatment with 10 μM phenformin and increasing concentrations of aspartate (mean ± SD, n = 3).

(F) Expression of an sgRNA-resistant GOT1 cDNA rescues the ETC inhibitor sensitivity of GOT1-null Jurkat cells. Fold change in cell number (log_2) of wild-type (black), GOT1-null (blue), and rescued GOT1-null (gray) cells after a 5-day treatment with antimycin (1 μM) or piericidin (0.5 μM) (mean ± SD, for n = 3, **$p < 0.05$).

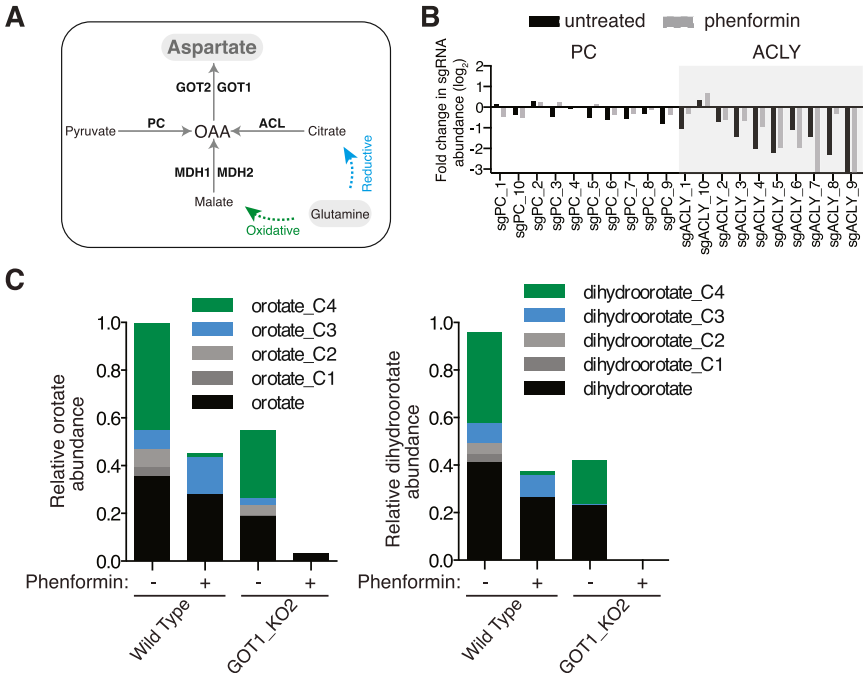

Figure S4. Aspartate Metabolism under ETC Inhibition, Related to Figure 4

(A) Metabolic pathways that lead to oxaloacetic acid (OAA) and aspartate production. In human cells, the primary carbon source for aspartate is oxaloacetate (OAA). OAA can be generated by multiple metabolic reactions. One source of OAA is through the malate dehydrogenases present in cytosol (MDH1) and mitochondria (MDH2). Second, pyruvate carboxylase can yield OAA from pyruvate in mitochondria. Finally, another source for OAA is through ATP-citrate lyase, which catalyzes the conversion of citrate and CoA into acetyl-CoA and OAA in cytoplasm. Citrate and malate can be derived from glutamine through reductive and oxidative pathways, respectively.

(B) Changes in abundance in the primary screen for individual PC and ACLY sgRNAs in the presence (gray) or absence (black) of phenformin.

(C) Upon ETC inhibition, nucleotide precursors are mainly synthesized by reductive metabolism of glutamine in a GOT1-dependent manner. Mass isotopomer analysis of orotate and dihydroorotate in wild-type and GOT1-null Jurkat cells cultured for 7 hr with [U-^{13}C]-L-glutamine in the presence or absence of phenformin (10 μM). (mean ± SD, for n = 3). OAA, oxaloacetate.

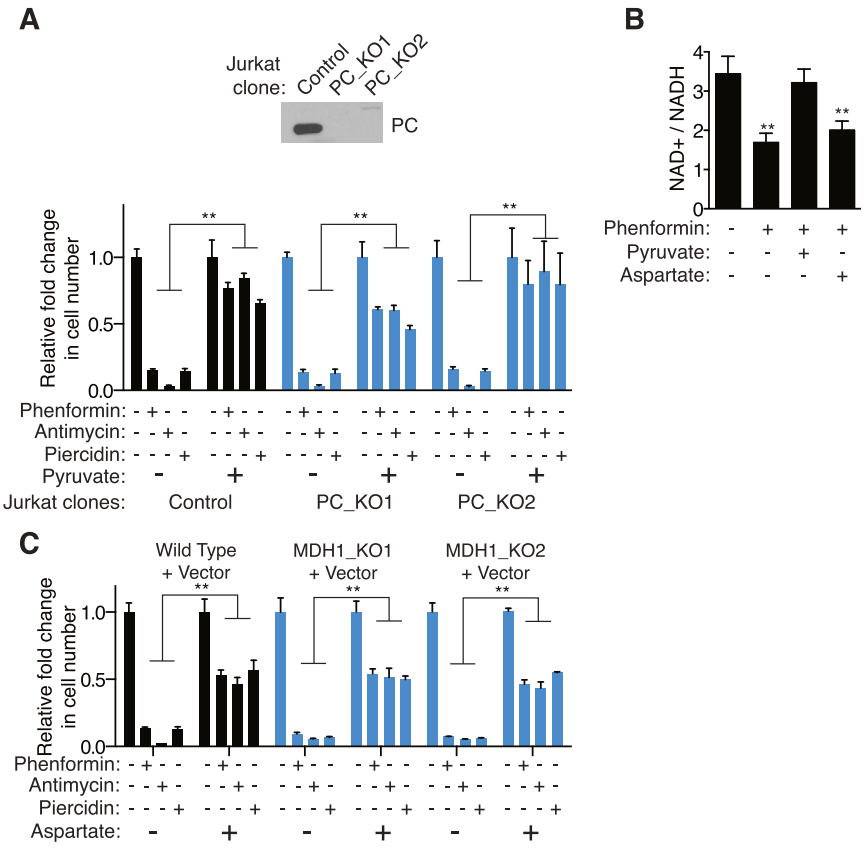

Figure S5. Cells with ETC Inhibition Does Not Require PC for Pyruvate to Enable Proliferation, Related to Figure 6

(A) Pyruvate can rescue the death of PC-null cells induced by ETC inhibition. Immunoblot analysis of wild-type and GOT1-null Jurkat cells (top). Relative fold change in cell number of wild-type (black) and PC-null (blue) Jurkat cells in the presence or absence of pyruvate (1 mM) after a 5-day treatment with phenformin (10 μM), antimycin (1 μM), or piericidin (0.5 μM) (mean ± SD, n = 3, **p < 0.05).

(B) Unlike pyruvate, aspartate does not increase the NAD+/NADH ratio in cells with ETC inhibition. NAD+/NADH ratio was determined for wild-type Jurkat cells after 24 hr phenformin treatment (10 μM) in the presence or absence of pyruvate (1 mM) or aspartate (10 mM) (mean ± SD, for n = 3, **p < 0.05).

(C) Aspartate can rescue the death of MDH1-null cells induced by ETC inhibition. Relative fold change in cell number of wild-type (black) and MDH1-null (blue) Jurkat cells in the presence or absence of aspartate (10 mM) after a 5-day treatment with phenformin (10 μM), antimycin (1 μM), or piericidin (0.5 μM) (mean ± SD, n = 3, **p < 0.05).

Cell

Supplemental Information

An Essential Role of the Mitochondrial Electron Transport Chain in Cell Proliferation Is to Enable Aspartate Synthesis

Kıvanç Birsoy, Tim Wang, Walter Chen, Elizaveta Freinkman, Monther Abu-Remaileh, and David M. Sabatini

Supplemental Experimental Procedures

Cell lines, constructs and antibodies

Materials were obtained from the following sources: antibodies to GOT1 from Novus (NBP1-54778), to MDH1 from Proteintech (15904-1-AP), to PC from Novus (NBP1-49536), to Raptor, mTOR, and pan-Akt from Cell Signaling Technologies; HRP-conjugated anti-rabbit antibody from Santa Cruz; Cell-Tak from BD Biosciences; sodium pyruvate, aspartic acid, polybrene, puromycin from Sigma; and blasticidin from Invivogen.

The Jurkat and Raji cell lines were purchased from ATCC and KMS-26 cells from the JCRB Cell Bank. 143B ρ^0, wild type, and CYTB cybrids were kindly provided by Navdeep Chandel (Northwestern University). MERRF cybrids were kindly provided by Giovanni Manfredi (Kwong et al., 2007; Wallace et al., 1988). All cell lines were grown in RPMI base medium containing 10% heat inactivated fetal bovine serum, 1 mM glutamine, penicillin, and streptomycin, unless otherwise indicated. For tracing experiments, RPMI without glucose and glutamine (US Biologicals-R9011), dialyzed fetal bovine serum (Sigma) and [U-^{13}C]-L-glutamine (CIL, CLM-1822-H-PK) were used. For cybrid and 143B ρ^0 proliferation experiments, RPMI without amino acids (US Biologicals-R8999) was used. Mouse embryonic fibroblasts were cultured in DMEM with 10% heat inactivated fetal bovine serum. Individual amino acids were reconstituted to RPMI amino acid concentrations except for aspartate and asparagine for the experiment in Figure 7D.

The lentiviral sgGOT1, sgMDH1 and sgPC vectors were generated via ligation of hybridized oligos (below) into lentiCRISPR-v1 vector linearized with BsmBI using Gibson assembly (NEB).

sgGOT1_10F, caccgGATAGGCTGAGTCAAAGAAG
sgGOT1_10R, AAACCTTCTTTGACTCAGCCTATCC
sgMDH1_1F, caccgGACATCTGGATACTGAGTCG
sgMDH1_1R, aaacCGACTCAGTATCCAGATGTCc
sgPC_1R, caccgCAGGCCCGGAACACACGGA
sgPC_1R, aaacTCCGTGTGTTCCGGGCCTGc

The retroviral *GOT1 and MDH1* vectors were generated by cloning sgGOT1_10 and sgMDH1_1 resistant GOT1 and MDH1 cDNAs synthesized by IDT (Geneblock) into the pMXS-ires-blast vector via Gibson Assembly. The retroviral *SLC1A3* vector was generated by cloning an SLC1A3 PCR fragment into the pMXS-ires-blast vector by Gibson Assembly. Primers for SLC1A3 PCR are below.

SLC1A3F,GCCGGATCTAGCTAGTTAATTAAGccaccATGACTAAAAGCAATGGAGA AGAGCCC;
SLC1A3R, GGGCGGAATTTACGTAGCCTACATCTTGGTTTCACTGTCGATGGG

CRISPR screens

The metabolism-focused sgRNA library was designed as previously described . Oligonucleotides for sgRNAs were synthesized by CustomArray Inc. and amplified by PCR (Wang et al., 2014). Amplicons were inserted into lentiCRISPR-v1, linearized by BsmBI digestion, by Gibson Assembly (NEB). Gibson Assembly products were then transformed into E. coli 10G SUPREME electrocompetent cells (Lucigen). This plasmid pool was used to generate lentivirus-containing supernatants. The titer of lentiviral supernatants was determined by infecting targets

cells at several amounts of virus in the presence of polybrene (4 ug/ml), counting the number of drug resistant infected cells after 3 days of selection. 40 million target cells were infected at an MOI of ~0.5 and selected with puromycin (4 ug/ml) 72 hours after infection. An initial pool of 40 million cells was harvested for genomic DNA extraction. The remaining cells were cultured for 14 doublings (with/without phenformin), after which cells were harvested for genomic DNA extraction. sgRNA inserts were PCR amplified, purified and sequenced on a HiSeq 2500 (Illumina) (primer sequences provided below). Sequencing reads were mapped and the abundance of each sgRNA was tallied. Gene score is defined as the median log2 fold change in the abundance between the initial and final population of all sgRNAs targeting that gene. The differential gene score is the difference between the untreated and phenformin-treated gene scores.

PCR primers for library amplification:
F-GGCTTTATATATCTTGTGGAAAGGACGAAACACCG
R-CTAGCCTTATTTTAACTTGCTATTTCTAGCTCTAAAAC
Primer sequences for sgRNA quantification are:
F-AATGATACGGCGACCACCGAGATCTAGAATACTGCCATTTGTCTCAAG
R-CAAGCAGAAGACGGCATACGAGATCnnnnnnTTTCTTGGGTAGTTTGCAGTTTT
(nnnnn denotes the sample barcode).
Illumina sequencing primer
isCGGTGCCACTTTTTCAAGTTGATAACGGACTAGCCTTATTTTAACTTGCTATTT
CTA GCTCTAAAAC.
Illumina indexing primer
isTTTCAAGTTACGGTAAGCATATGATAGTCCATTTTAAAACATAATTTTAAAACTG
CAA ACTACCCAAGAAA.

Seahorse measurements
Oxygen consumption of intact cells was measured using an XF24 Extracellular Flux Analyzer (Seahorse Bioscience). For Jurkat cells, seahorse plates were coated with Cell TAK (BD, 0.02 mg/ml in 0.1 μM $NaHO_3$) for 20 minutes to increase adherence of suspension cells. 200,000 cells were then attached to the plate by centrifugation at 2,200 rpm without brakes for 5 min. RPMI 8226 (US biological #9011) assay media was used as previously described (Birsoy et al., 2014). For basal oxygen consumption measurements the cell number was used to normalize. In order to increase phenformin entry, OCR measurements were taken 20 minutes after phenformin injection.

Gene set enrichment analysis
To study the association of gene sets with sensitivity to phenformin, we used the GSEA tool developed by the Broad Institute (Subramanian et al., 2005). The enrichment scores (ES) were computed for the ranked genes from the phenformin screen.

NAD^+ and NADH measurements:
The NAD+/NADH ratio was measured by modification of manufacturer instructions for NAD^+/NADH Glo Assay (Promega). Jurkat cells were incubated in RPMI under the conditions listed for 8 hours before cell extracts were taken. To extract

NAD^+/NADH, cells were centrifuged for 1 minute at 300 x g, and washed 3 times by quickly resuspending in 15 mL PBS and centrifuging for 1 minute at 300 x g. Pelleted samples were extracted in 100 µL ice cold lysis buffer (1% Dodecyltrimethylammonium bromide (DTAB) in 0.2 N NaOH diluted 1:1 with PBS) and frozen at -80°C. To measure NADH, 20 µL of extracts were heated to 75°C for 30 min in the basic lysis buffer to degrade NAD^+. To measure NAD^+, samples were diluted 1:1 with 0.4 N HCl and incubated at 60°C for 15 min where acidic conditions will degrade NADH. Following incubations, samples were quenched by adding 20 µL of 0.25 M Tris, 0.2 N HCl (NADH) or 20 µL of 0.5 M Tris base (NAD^+). Manufacturer instructions were then followed to measure NAD^+/NADH.

Immunoblotting

1.5 million Jurkat cells were rinsed twice in ice-cold PBS and harvested in a standard lysis buffer containing 50 mM Hepes, pH 7.4, 40 mM NaCl, 2 mM EDTA, 1.5 mM orthovanadate, 50 mM NaF, 10 mM pyrophosphate, 10 mM glycerophosphate, protease inhibitors (Roche) and 1% Triton-X-100. Proteins from total lysates were resolved by 12% SDS-PAGE, and analyzed by immunoblotting as described (Birsoy et al., 2014).

Mouse studies

All animal studies and procedures were approved by the MIT Institutional Animal Care and Use Committee. *TFAM*$^{loxP/loxP}$ mice were a generous gift from Dr. Navdeep Chandel and were generated as described previously (Larsson et al., 1998). *Ckmm-Cre/+* B6.FVB(129S4-Tg(Ckmm-cre)5Khn/J mice were obtained from The Jackson Laboratory and mated to *TFAM*$^{loxP/loxP}$ mice to generate *Ckmm-Cre/+, TFAM*$^{loxP/loxP}$ mice. All mice were maintained on a standard light-dark cycle with food and water *ad libitum*. Genotyping primers were designed to distinguish between the native wild type and loxP-containing alleles: mTFAMF1, CTGCCTTCCTCTAGCCCGGG; mTFAMR1, GTAACAGCAGACAACTTGTG; mTFAMR2, CTCTGAAGCACATGGTCAAT. When all three primers are included in the genotyping reaction, a wild type and loxP-containing allele produce a 404 and 437 bp band, respectively. Hearts were isolated from 14-16 week old animals and amino acid levels were determined from lysates as described above.

References

Birsoy, K., Possemato, R., Lorbeer, F.K., Bayraktar, E.C., Thiru, P., Yucel, B., Wang, T., Chen, W.W., Clish, C.B., and Sabatini, D.M. (2014). Metabolic determinants of cancer cell sensitivity to glucose limitation and biguanides. Nature *508*, 108-112.

Kwong, J.Q., Henning, M.S., Starkov, A.A., and Manfredi, G. (2007). The mitochondrial respiratory chain is a modulator of apoptosis. The Journal of cell biology *179*, 1163-1177.

Larsson, N.G., Wang, J., Wilhelmsson, H., Oldfors, A., Rustin, P., Lewandoski, M., Barsh, G.S., and Clayton, D.A. (1998). Mitochondrial transcription factor A is necessary for mtDNA maintenance and embryogenesis in mice. Nature genetics *18*, 231-236.

Subramanian, A., Tamayo, P., Mootha, V.K., Mukherjee, S., Ebert, B.L., Gillette, M.A., Paulovich, A., Pomeroy, S.L., Golub, T.R., Lander, E.S.*, et al.* (2005). Gene set enrichment analysis: a knowledge-based approach for interpreting genome-wide expression profiles. Proceedings of the National Academy of Sciences of the United States of America *102*, 15545-15550.

Wallace, D.C., Zheng, X.X., Lott, M.T., Shoffner, J.M., Hodge, J.A., Kelley, R.I., Epstein, C.M., and Hopkins, L.C. (1988). Familial mitochondrial encephalomyopathy (MERRF): genetic, pathophysiological, and biochemical characterization of a mitochondrial DNA disease. Cell *55*, 601-610.

Wang, T., Wei, J.J., Sabatini, D.M., and Lander, E.S. (2014). Genetic screens in human cells using the CRISPR-Cas9 system. Science *343*, 80-84.